

# Experimental and Theoretical Study of the Regiospecific Coordination of Ru<sup>II</sup> and Os<sup>II</sup> Fragments on the Lacunary Polyoxometalate [ $\alpha$ -PW<sub>11</sub>O<sub>39</sub>]<sup>7-</sup>

Danielle Laurencin,<sup>†</sup> Richard Villanneau,<sup>†</sup> H el ene G erard,<sup>\*,‡</sup> and Anna Proust<sup>\*,†</sup>

Laboratoire de Chimie Inorganique et Mat eriaux Mol eculaires, UMR 7071, Universit e Pierre et Marie Curie, Case 42, 4 place Jussieu, 75252 Paris Cedex 05, France, and Laboratoire de Chimie Th eorique, UMR 7616, Universit e Pierre et Marie Curie, Case 137, 4 place Jussieu, 75252 Paris Cedex 05, France

Received: November 24, 2005; In Final Form: March 22, 2006

New Ru<sup>II</sup> and Os<sup>II</sup> derivatives of the monovacant [ $\alpha$ -PW<sub>11</sub>O<sub>39</sub>]<sup>7-</sup> anion ([PW<sub>11</sub>O<sub>39</sub>{M(DMSO)<sub>3</sub>(H<sub>2</sub>O)}]<sup>5-</sup> (M = Ru (**1**), Os (**2**)) and [PW<sub>11</sub>O<sub>39</sub>{Os( $\eta^6$ -*p*-cym)(H<sub>2</sub>O)}]<sup>5-</sup> (**3**)) have been synthesized and characterized. The binding mode of the d<sup>6</sup>-{M<sup>II</sup>L<sub>3</sub>(H<sub>2</sub>O)}<sup>2+</sup> moieties in these compounds is similar to that in the previously described [PW<sub>11</sub>O<sub>39</sub>{Ru( $\eta^6$ -*p*-cym)(H<sub>2</sub>O)}]<sup>5-</sup> (**4**) complex: bidentate, on two nonequivalent oxygen atoms of the lacuna, leading to a loss of the C<sub>s</sub> symmetry of the parent anion, which thus plays the role of a prochiral bidentate ligand. The density functional theory (DFT) (B3PW91) computation of the lowest unoccupied molecular orbitals of the {ML<sub>3</sub>(H<sub>2</sub>O)}<sup>2+</sup> (M = Os, Ru; L<sub>3</sub> = *fac*-(DMSO)<sub>3</sub>,  $\eta^6$ -C<sub>6</sub>H<sub>6</sub>) fragments reveals the similarities between their electrophilic properties. The origin of the regioselectivity of the grafting was investigated through a DFT (B3PW91) analysis of (i) the highest occupied molecular orbital of [ $\alpha$ -PW<sub>11</sub>O<sub>39</sub>]<sup>7-</sup> and (ii) the relative energies of the different potential regioisomers obtained by a bidentate grafting of the {ML<sub>3</sub>(H<sub>2</sub>O)}<sup>2+</sup> moiety onto the lacuna of [ $\alpha$ -PW<sub>11</sub>O<sub>39</sub>]<sup>7-</sup>. The role of the water ligand in the stabilization of this peculiar structure was studied.

## 1. Introduction

During the past two decades, several teams have focused their research on the development of environmentally friendly procedures.<sup>1</sup> In this context, the synthesis of water soluble catalysts has attracted continuously growing attention, as can be seen by the number of complexes described in the literature. The solubility of such compounds in water results from the coordination of one or several hydrophilic ligands on the transition metal cation.<sup>2–7</sup>

Among the different potential water soluble ligands, polyoxometalates (POMs) naturally appear as interesting. Indeed, an important number of polyoxoanions are rigid, thermally robust, and nonsensitive to oxidation.<sup>8</sup> Their coordination chemistry with transition metal cations has thus been particularly well documented.<sup>8,9</sup> In particular, many transition metals have been incorporated in the monolacunary Keggin anions of the general formula [ $\alpha$ -XW<sub>11</sub>O<sub>39</sub>]<sup>n-</sup> (X = P, n = 7; X = Ge, Si, n = 8). The analysis of the different structures obtained underscores the versatility of this inorganic ligand. In most cases, it behaves as a pentadentate ligand, by coordination of the metal to all four oxygen atoms of the lacuna and to one oxygen atom of the central [XO<sub>4</sub>]<sup>p-</sup> moiety, for example, in the structures [ $\alpha$ -PW<sub>11</sub>O<sub>39</sub>{Co(H<sub>2</sub>O)}]<sup>4-</sup> and [ $\alpha$ -PW<sub>11</sub>O<sub>39</sub>{Ti(Cp)}]<sup>4-</sup> (Cp = cyclopentadienyl).<sup>8e,10</sup> In other cases, the metal is coordinated to only two oxygen atoms of the lacuna, for example, in the [ $\alpha$ -PW<sub>11</sub>O<sub>39</sub>{Rh<sub>2</sub>(OAc)<sub>2</sub>(DMSO)<sub>2</sub>}]<sup>5-</sup> (AcO<sup>-</sup> = acetate, DMSO = S-bonded dimethyl sulfoxide).<sup>11</sup>

Among the numerous transition metals which are likely to be incorporated in polyoxometalates, ruthenium appeared from the start to be particularly attractive, because of the great

catalytic potential of this metal,<sup>12</sup> and many structures have thus been obtained. Moreover, the incorporation of ruthenium fragments in [ $\alpha$ -XW<sub>11</sub>O<sub>39</sub>]<sup>n-</sup> structures illustrates perfectly the different binding abilities of this polyoxoanionic framework: as shown in Figure 1, the lacunary POM either serves as a bidentate ligand, for example, in [ $\alpha$ -PW<sub>11</sub>O<sub>39</sub>{Ru( $\eta^6$ -arene)(H<sub>2</sub>O)}]<sup>5-</sup> (arene = benzene, toluene, *p*-cymene, hexamethylbenzene)<sup>13</sup> or as a pentadentate ligand, for example, in [ $\alpha$ -PW<sub>11</sub>O<sub>39</sub>{Ru<sup>II</sup>(DMSO)}]<sup>5-</sup>.<sup>14,15</sup> In the former structure, it is noteworthy that the {RuL<sub>3</sub>(H<sub>2</sub>O)}<sup>2+</sup> fragment is bound to two nonequivalent oxygen atoms of the lacuna, leading to a loss of the C<sub>s</sub> symmetry of the parent anion [ $\alpha$ -PW<sub>11</sub>O<sub>39</sub>]<sup>7-</sup>, according to X-ray and <sup>183</sup>W NMR studies. The study of the origin of these singular properties of [ $\alpha$ -XW<sub>11</sub>O<sub>39</sub>]<sup>n-</sup> ligands has however never been undertaken so far.

In the following report, an investigation of the binding ability of [ $\alpha$ -PW<sub>11</sub>O<sub>39</sub>]<sup>7-</sup> toward the Ru<sup>II</sup> fragments {Ru(DMSO)<sub>3</sub>(H<sub>2</sub>O)}<sup>2+</sup> and {Ru( $\eta^6$ -arene)(H<sub>2</sub>O)}<sup>2+</sup> and the Os<sup>II</sup> fragments {Os(DMSO)<sub>3</sub>(H<sub>2</sub>O)}<sup>2+</sup> and {Os( $\eta^6$ -arene)(H<sub>2</sub>O)}<sup>2+</sup> is proposed. First, from an experimental point of view, the syntheses of [ $\alpha$ -PW<sub>11</sub>O<sub>39</sub>{Ru(DMSO)<sub>3</sub>(H<sub>2</sub>O)}]<sup>5-</sup> (**1**), [ $\alpha$ -PW<sub>11</sub>O<sub>39</sub>{Os(DMSO)<sub>3</sub>(H<sub>2</sub>O)}]<sup>5-</sup> (**2**), and [ $\alpha$ -PW<sub>11</sub>O<sub>39</sub>{Os( $\eta^6$ -*p*-cym)(H<sub>2</sub>O)}]<sup>5-</sup> (**3**) (*p*-cym = *p*-cymene) are described. Then, a DFT study is reported (i) to investigate by an orbital approach the regioselectivity of the bidentate grafting of {ML<sub>3</sub>(H<sub>2</sub>O)}<sup>2+</sup> moieties (M = Ru, Os; L<sub>3</sub> = *fac*-(DMSO)<sub>3</sub>,  $\eta^6$ -arene) on [ $\alpha$ -PW<sub>11</sub>O<sub>39</sub>]<sup>7-</sup> and (ii) to analyze the energetic and structural factors involved during the grafting of these electrophilic fragments on the lacuna.

## 2. Experimental Section

**Materials and Methods.** The K<sub>7</sub>[ $\alpha$ -PW<sub>11</sub>O<sub>39</sub>]<sup>7-</sup>·14H<sub>2</sub>O,<sup>16</sup> *fac*-[RuCl<sub>2</sub>(DMSO)<sub>3</sub>(DMSO)],<sup>17</sup> *fac*-[OsCl<sub>2</sub>(DMSO)<sub>3</sub>(DMSO)],<sup>18</sup> and [Os( $\eta^6$ -*p*-cym)Cl<sub>2</sub>]<sub>2</sub><sup>19</sup> complexes were prepared as described in the literature. All other reagents were obtained from commercial sources and used as received. IR spectra were recorded from

\* To whom correspondence should be addressed. E-mail: gerard@lct.jussieu.fr; proust@ccr.jussieu.fr.

<sup>†</sup> Laboratoire de Chimie Inorganique et Mat eriaux Mol eculaires.

<sup>‡</sup> Laboratoire de Chimie Th eorique.

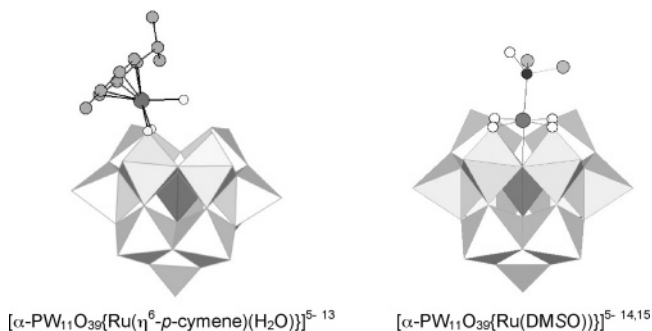


**Figure 1.** Two modes of coordination of ruthenium on the  $[\alpha\text{-PW}_{11}\text{O}_{39}]^{7-}$  anion.

KBr pellets on a Bio-Rad RT 165 spectrometer. The  $^1\text{H}$  (300.13 MHz, TMS) and  $^{31}\text{P}$  (121.5 MHz, external 85%  $\text{H}_3\text{PO}_4$ ) NMR spectra were obtained in solution on a Bruker AC 300 spectrometer equipped with a QNP probehead. The  $^{13}\text{C}$ - $^1\text{H}$  HSQC NMR spectrum of **1** was recorded on a Bruker Avance DMX500 spectrometer, operating at a  $^1\text{H}$  resonance frequency of 500.13 MHz and using the standard Bruker software.<sup>20</sup>

**Synthesis of  $\text{Cs}_{5-x}\text{K}_x[\alpha\text{-PW}_{11}\text{O}_{39}\{\text{Ru}(\text{DMSO})_3(\text{H}_2\text{O})\}]$  ( $\text{Cs}_{5-x}\text{K}_x\text{-1}$ ).** A mixture of  $\text{K}_7[\alpha\text{-PW}_{11}\text{O}_{39}]\cdot 14\text{H}_2\text{O}$  (0.546 g, 0.17 mmol) and of *fac*- $[\text{RuCl}_2(\text{DMSO})_3(\text{DMSO})]$  (0.081 g, 0.17 mmol) in 7 mL of water was refluxed for 1 h, then left to cool at room temperature.<sup>21a</sup> At this stage, according to the  $^{31}\text{P}$  NMR spectrum of the solution, one main product, **1**, was present ( $\delta = -11.01$  ppm, 76%), along with several minor species ( $\delta = -9.98, -10.44, -11.28, -12.01$  ppm). The corresponding  $^1\text{H}$  and  $^{13}\text{C}$  NMR spectra (obtained after reaction in  $\text{D}_2\text{O}$ ) each display six singlets of equal intensity and one singlet which can be attributed to free DMSO ( $\delta(\text{OS}(\text{CH}_3)_2) = 2.71$  ppm,  $\delta(\text{OS}(\text{CH}_3)_2) = 39.39$  ppm); correspondence between the  $^1\text{H}$  and  $^{13}\text{C}$  signals could be made by recording the HSQC NMR spectrum of the mother liquor; the two-dimensional NMR spectrum is represented in the Supporting Information.  $\text{CsCl}$  (0.417 g, 2.48 mmol, 15 equiv) was then added to the solution, leading to the precipitation of an orange solid which was separated by filtration and identified as a fairly pure sample of  $\text{Cs}_{5-x}\text{K}_x[\alpha\text{-PW}_{11}\text{O}_{39}\{\text{Ru}(\text{DMSO})_3(\text{H}_2\text{O})\}]$  ( $\text{Cs}_{5-x}\text{K}_x\text{-1}$ ) (0.474 g). IR (KBr,  $\text{cm}^{-1}$ ): 3010 (w), 2928 (w), 1407 (w), 1319 (w), 1300 (w), 1261 (w), 1116 (sh), 1092 (m), 1040 (m), 1021 (sh), 951 (s), 890 (s), 848 (s), 809 (s), 731 (s), 515 (w), 428 (w), 369 (m).  $^1\text{H}$  NMR ( $\text{D}_2\text{O}$ ):  $\delta = 3.17, 3.44, 3.56, 3.68, 3.78, 3.83$  ppm (all singlets with equal intensities).  $^{13}\text{C}$  NMR ( $\text{D}_2\text{O}$ ):  $\delta = 44.15, 45.21, 45.24, 45.50, 46.67, 46.86$  ppm (all singlets with equal intensities).  $^{31}\text{P}$  NMR ( $\text{D}_2\text{O}$ ):  $\delta = -11.01$  ppm.<sup>21b</sup>

**Formation of  $\text{Cs}_{5-x}\text{K}_x[\alpha\text{-PW}_{11}\text{O}_{39}\{\text{Os}(\text{DMSO})_3(\text{H}_2\text{O})\}]$  ( $\text{Cs}_{5-x}\text{K}_x\text{-2}$ ).** A mixture of  $\text{K}_7[\alpha\text{-PW}_{11}\text{O}_{39}]\cdot 14\text{H}_2\text{O}$  (0.321 g, 0.10 mmol) and *fac*- $[\text{OsCl}_2(\text{DMSO})_3(\text{DMSO})]$  (0.057 g, 0.10 mmol) in 7 mL of  $\text{D}_2\text{O}$  was refluxed for 1 h, then left to cool at room temperature. At this stage, according to the  $^{31}\text{P}$  NMR spectrum of the solution, one main product, **2**, was present ( $\delta = -11.21$  ppm, 52%), along with a few minor species ( $\delta = -10.18, -10.71, -11.48, -12.21$  ppm). On the corresponding  $^1\text{H}$  NMR spectrum, apart from the five main singlets of relative intensities 1:1:1:1:2 and one singlet due to free DMSO, a broad signal ( $\Delta\nu = 80$  Hz) could also be detected, suggesting that some  $\text{Os}^{\text{II}}$  fragments could have been oxidized to  $\text{Os}^{\text{III}}$ .  $\text{CsCl}$  (0.253 g, 1.50 mmol, 15 equiv) was then added, leading to the precipitation of an orange solid which was separated by filtration, dried with diethyl ether, and identified as an impure sample of  $\text{Cs}_{5-x}\text{K}_x[\alpha\text{-PW}_{11}\text{O}_{39}\{\text{Os}(\text{DMSO})_3(\text{H}_2\text{O})\}]$  ( $\text{Cs}_{5-x}\text{K}_x\text{-2}$ ) (0.150 g). The new fraction of orange solid which had formed in the

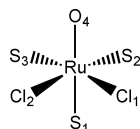
filtrate was separated by filtration, dried with diethyl ether, and identified as a more pure sample of **2** (yield: 0.050 g). IR (KBr,  $\text{cm}^{-1}$ ): 3017 (w), 2920 (w), 1419 (w), 1320 (w), 1300 (w), 1119 (sh), 1087 (m), 1045 (m), 1019 (sh), 948 (s), 889 (s), 847 (s), 806 (s), 742 (s), 512 (w), 433 (w), 365 (m).  $^1\text{H}$  NMR ( $\text{D}_2\text{O}$ ):  $\delta = 3.25, 3.56, 3.66, 3.71, 3.90$  ppm (all singlets with relative intensities 1:1:1:1:2).  $^{31}\text{P}$  NMR ( $\text{D}_2\text{O}$ ):  $\delta = -11.21$  ppm.

**Formation of  $\text{Cs}_{5-x}\text{K}_x[\alpha\text{-PW}_{11}\text{O}_{39}\{\text{Os}(\eta^6\text{-}p\text{-cym})(\text{H}_2\text{O})\}]$  ( $\text{Cs}_{5-x}\text{K}_x\text{-3}$ ).** A suspension of  $[\text{Os}(\eta^6\text{-}p\text{-cym})\text{Cl}_2]_2$  (0.085 g, 0.11 mmol, 1.2 equiv) and  $\text{K}_7[\alpha\text{-PW}_{11}\text{O}_{39}]\cdot 14\text{H}_2\text{O}$  (0.576 g, 0.18 mmol, 1 equiv) in 7 mL of  $\text{D}_2\text{O}$  was refluxed for 45 min, leading to the formation of a unique species **3**, as attested by the  $^{31}\text{P}$  and  $^1\text{H}$  NMR spectra of the mother liquor (see the Supporting Information).<sup>22</sup> The compound was precipitated by the addition of cesium chloride (0.140 g, 4.6 equiv), separated by filtration, and identified as  $\text{Cs}_{5-x}\text{K}_x[\alpha\text{-PW}_{11}\text{O}_{39}\{\text{Os}(\eta^6\text{-}p\text{-cym})(\text{H}_2\text{O})\}]$  ( $\text{Cs}_{5-x}\text{K}_x\text{-3}$ ) (yield: 0.110 g).<sup>23</sup> IR (KBr,  $\text{cm}^{-1}$ ): 3056 (w), 2962 (w), 2924 (w), 2870 (w), 1471 (w), 1387 (w), 1100 (m), 1043 (m), 950 (s), 886 (m), 844 (s), 805 (s), 761 (w), 597 (w), 512 (m), 374 (m), 334 (m).  $^1\text{H}$  NMR ( $\text{D}_2\text{O}$ ):  $\delta = 1.45$  (d,  $^3J = 3.0$  Hz, 3H; Ar- $\text{CH}(\text{CH}_3)_2$ ), 1.48 (d,  $^3J = 3.0$  Hz, 3H; Ar- $\text{CH}(\text{CH}_3)_2$ ), 2.61 (s, 3H; Ar- $\text{CH}_3$ ), 3.01 (m, 1H; Ar- $\text{CH}(\text{CH}_3)_2$ ), 6.40 (d,  $^3J = 6.1$ , 1H; Ar-*H*), 6.55 (d,  $^3J = 4.8$ , 1H; Ar-*H*), 6.71 (d,  $^3J = 5.0$ , 1H; Ar-*H*), 6.90 ppm (d,  $^3J = 5.5$ , 1H; Ar-*H*).  $^{31}\text{P}$  NMR ( $\text{D}_2\text{O}$ ):  $\delta = -12.27$  ppm.<sup>24</sup>

**Computational Details.** Calculations on the metal fragments  $\{\text{Ru}(\text{DMSO})_3(\text{H}_2\text{O})\}^{2+}$ ,  $\{\text{Ru}(\eta^6\text{-C}_6\text{H}_6)(\text{H}_2\text{O})\}^{2+}$ ,  $\{\text{Os}(\text{DMSO})_3(\text{H}_2\text{O})\}^{2+}$ , and  $\{\text{Os}(\eta^6\text{-C}_6\text{H}_6)(\text{H}_2\text{O})\}^{2+}$  were carried out with the GAUSSIAN-98 set of programs<sup>25</sup> within the framework of the DFT, using the B3PW91 functional.<sup>26</sup> The LANL2DZ effective core potentials were used to replace the 10 core electrons of S and the 28 innermost electrons of Ru.<sup>27a,b</sup> The associated double  $\zeta$  basis set was used and was augmented by a d polarization function for S.<sup>27c</sup> The SDD effective core potential was used to replace the 60 innermost electrons of Os,<sup>28</sup> and the associated double  $\zeta$  basis set was used. A 6-31G\*\* basis set was used for all other elements. Further discussions about the accuracy of this methodological choice are carried out below. The geometries used in the orbital computation of the  $\{\text{ML}_3(\text{H}_2\text{O})\}^{2+}$  (M = Ru, Os) fragments were derived from the fully optimized geometry of the *fac*- $[\text{ML}_3(\text{H}_2\text{O})(\text{OH})_2]$  complex, in which the fragment is associated with two hydroxo ligands to mimic the coordination of the ruthenium and osmium to two oxygen atoms of the lacuna of  $[\alpha\text{-PW}_{11}\text{O}_{39}]^{7-}$ .

Calculations on the lacunary POM  $[\alpha\text{-PW}_{11}\text{O}_{39}]^{7-}$  and on its  $\text{Ru}^{\text{II}}$  derivatives were carried out using the Jaguar 6.0 release 11 set of programs,<sup>29</sup> within the framework of the DFT using the B3PW91 functional. The LANL2DZ effective core potentials were used to replace the 60 innermost electrons of W, the 28 innermost electrons of Ru and the 10 innermost electrons of P. The associated double  $\zeta$  basis set was used for these atoms, and a 6-31+G\* basis set was used for the other atoms. Full geometry optimization was carried out, except when otherwise specified. Solvation was taken into account by using the JAGUAR self-consistent reaction field continuum dielectric.<sup>30</sup> Parameters were chosen to model water (dielectric constant equal to 80.37).

**Choice of Functional and Basis Set.** With the main target being the study of the bidentate coordination of ruthenium fragments on the POM, a good description of the electronic structure of this metal appeared to be necessary: we thus first investigated the effect of the functional and the basis set on the

**TABLE 1:** Effect of the Choice of the Functional and Basis Set on the Ruthenium–Ligand Bond Distances and on the S–O Frequencies of the DMSO Ligands. The Numbering Used for the Atoms Coordinated to the Ru Is the One Represented Below

Methods and Basis Sets						
	1	2	3	4	5	
functional	B3LYP	B3LYP	B3LYP	BP86	B3PW91	
H, C, O	6-31G**	6-31+G**	6-31G**	6-31G**	6-31G**	
S	LANL2DZ/d	6-31+G**	LANL2DZ/d	LANL2DZ/d	LANL2DZ/d	
Cl	LANL2DZ/d	6-31+G**	LANL2DZ/d	LANL2DZ/d	LANL2DZ/d	
Ru	LANL2DZ	LANL2DZ	LANL2DZ/f	LANL2DZ	LANL2DZ	
Bond Lengths (Å)						
distance	RX <sup>17c</sup>	1	2	3	4	5
Ru···S <sub>1</sub>	2.252(1)	2.3448	2.3547	2.3354	2.2997	2.3097
Ru···S <sub>2</sub>	2.277(1)	2.3737	2.3904	2.3632	2.3431	2.3305
Ru···S <sub>3</sub>	2.276(1)	2.3715	2.3864	2.3616	2.3111	2.3309
Ru···O <sub>4</sub>	2.142(3)	2.1946	2.2071	2.1885	2.1819	2.1798
Ru···Cl <sub>1</sub>	2.435(1)	2.4860	2.4817	2.4788	2.4692	2.4586
Ru···Cl <sub>2</sub>	2.435(1)	2.4823	2.4830	2.4825	2.4587	2.4624
S–O Stretching Frequencies (cm <sup>-1</sup> )						
frequency	expt <sup>17b,c</sup>	1	2	3	4	5
DMSO	1095	1096	1084	1096	1037	1112
	1110	1103	1090	1103	1056	1119
	1122	1108	1095	1109	1072	1125
DMSO	921	891	893	889	852	908

calculations carried out on the *fac*-[RuCl<sub>2</sub>(DMSO)<sub>3</sub>(DMSO)] complex. The influence of the functional and basis set on both the structural parameters and the vibrational frequencies of *fac*-[RuCl<sub>2</sub>(DMSO)<sub>3</sub>(DMSO)] was considered. Indeed, even though the aim of our study is not to reproduce the spectroscopic characteristics of the ruthenium and osmium derivatives of POMs, the vibrational study of *fac*-[RuCl<sub>2</sub>(DMSO)<sub>3</sub>(DMSO)] was performed to probe the quality of reproduction of the electronic environment at the metal.

The effect of the basis was first examined using the B3LYP functional,<sup>26a,31</sup> which is the most widely used for transition metal complexes.<sup>32</sup> Results for all electron computations and a large basis (except for Ru; Table 1, entry 2) were compared with those obtained using effective core potentials for all heavy atoms (entry 1). No major geometric effect is observed, and the calculated bond distances are systematically found to be approximately 0.1 Å too long for the Ru···S bond lengths and over 0.05 Å too long for the Ru···O distances compared with the X-ray values. This problem could not be improved by adding an f polarization function on Ru<sup>27d</sup> (entry 3). Regarding the calculated S–O stretching frequencies, they are globally smaller than the experimental values and no effect of the polarization f orbital is observed (less than 1 cm<sup>-1</sup>). Using an all electron polarized basis set even worsens the discrepancy with the experimental frequencies (entry 2).

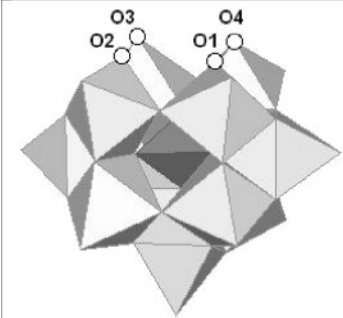
We thus tried to change the functional to better reproduce both geometrical and vibrational data and thus very probably improve the description of metal–ligand interactions. BP86 and B3PW91 computations were undertaken using the smaller basis set since no major effect had been found using B3LYP. The BP86 functional (entry 4),<sup>26,33</sup> which has been used in the past in the literature for the study of [RuCl<sub>2</sub>(DMSO)<sub>4</sub>] isomers,<sup>34</sup> gives better results as far as the bond lengths are concerned but much worse results for the S–O vibration frequencies. In the case of B3PW91 (entry 5), the obtained Ru···S and Ru···O

distances are substantially shorter than those obtained with B3LYP (but slightly longer than those obtained with BP86) and thus closer to the X-ray values. Furthermore, S–O vibrational frequencies increase compared with B3LYP and become higher than the experimental ones. This is of special interest to us since vibrational frequencies computed in the harmonic approximation are generally overestimated,<sup>35</sup> which made the smaller values obtained with B3LYP particularly disturbing. As for the S–O stretching frequency, the B3PW91 value is also the closest to the experimental value; further calculations were thus undertaken using the B3PW91 functional and the small basis set. They are indeed expected to better reproduce the coordination ability of the Ru moiety, since they properly reproduce its electronic environment, as probed from spectroscopic data.

Additional tests were carried out on the lacunary complex [ $\alpha$ -PW<sub>11</sub>O<sub>39</sub>]<sup>7-</sup> to evaluate the effect of the functional on the highest occupied molecular orbital (HOMO) as well as on the geometrical parameters of the lacuna. The HF, B3LYP, and B3PW91 aspects of the HOMO are identical, which is especially noteworthy since the HOMO-*x* orbitals are very close in energy to the HOMO. Furthermore, we evaluated the effect of the functional on the optimized geometry of the lacunary POM, for which the largest structural differences are expected. The four O···O distances between the oxygen atoms of the lacuna are given in Table 2. The discrepancies between two corresponding O···O distances are below 0.06 Å, which is rather small regarding that these distances are long and characteristic of nonbonding interactions. Consequently, since the grafted metal fragment is better described using B3PW91, this functional was chosen throughout this study for the computations on the POM. It should be noted that, in this work, the purpose of the calculations is to analyze the grafting properties of different electrophilic fragments on the lacunary POM and not to try to reproduce or simulate the experimental spectroscopic data of these compounds.



**TABLE 2: O...O Distances in the Optimized  $[\alpha\text{-PW}_{11}\text{O}_{39}]^{7-}$  Anion Depending on the Functional (distances are given in angstroms; the starting point geometry used for  $[\alpha\text{-PW}_{11}\text{O}_{39}]^{7-}$  was that extracted from the X-ray structure of  $[\alpha\text{-PW}_{11}\text{O}_{39}\{\text{Ru}(\eta^6\text{-}p\text{-cym})(\text{H}_2\text{O})\}]^{5-}$ )**

	Distance	B3LYP	B3PW91
	O <sub>1</sub> ...O <sub>2</sub>		3.28
O <sub>2</sub> ...O <sub>3</sub>		3.76	3.73
O <sub>3</sub> ...O <sub>4</sub>		3.53	3.50
O <sub>4</sub> ...O <sub>5</sub>		3.74	3.75

### 3. Characterizations of Compounds 1, 2, and 3

Following the experimental conditions for the synthesis of  $[\alpha\text{-PW}_{11}\text{O}_{39}\{\text{Ru}(\eta^6\text{-}p\text{-cym})(\text{H}_2\text{O})\}]^{5-}$  (**4**),<sup>13</sup>  $[\alpha\text{-PW}_{11}\text{O}_{39}\{\text{Ru}(\text{DMSO})_3(\text{H}_2\text{O})\}]^{5-}$  (**1**),  $[\alpha\text{-PW}_{11}\text{O}_{39}\{\text{Os}(\text{DMSO})_3(\text{H}_2\text{O})\}]^{5-}$  (**2**), and  $[\alpha\text{-PW}_{11}\text{O}_{39}\{\text{Os}(\eta^6\text{-}p\text{-cym})(\text{H}_2\text{O})\}]^{5-}$  (**3**) have been obtained by the reaction between  $\text{K}_7[\alpha\text{-PW}_{11}\text{O}_{39}] \cdot 14\text{H}_2\text{O}$  and either *fac*- $[\text{RuCl}_2(\text{DMSO})_3(\text{DMSO})]$ , *fac*- $[\text{OsCl}_2(\text{DMSO})_3(\text{DMSO})]$ , or  $[\text{Os}(\eta^6\text{-}p\text{-cym})\text{Cl}_2]_2$ , respectively, in an equimolar ratio in boiling water. Compounds **1–3** have been identified by <sup>31</sup>P NMR, <sup>1</sup>H NMR, and IR spectroscopies.

In each case, after 1 h of reflux in D<sub>2</sub>O, the <sup>31</sup>P NMR spectrum of the solution reveals the presence of one major product, whose chemical shift (−11.01 ppm for **1**, −11.21 ppm for **2**, and −12.27 ppm for **3**) is shifted toward lower frequency with respect to that of the free  $[\alpha\text{-PW}_{11}\text{O}_{39}]^{7-}$  anion (−10.44 ppm), which is in accord with the grafting of a metal fragment (i.e., a ruthenium or osmium fragment) onto the lacuna of the polyoxometalate.<sup>36</sup>

For **2** and **3**, the <sup>1</sup>H NMR spectra of the mother liquor reveal the presence of free DMSO in solution (meaning that DMSO molecules have decoordinated from the starting precursor),<sup>37,38</sup> and the chemical shift range of the remaining signals is typical for DMSO ligands coordinated via the sulfur atom to a Ru<sup>II</sup> or Os<sup>II</sup> center. The presence of six singlets of equal intensity for **1** suggests that there are three remaining S-bonded DMSO ligands on the ruthenium and that the six methyl groups are magnetically inequivalent (meaning that there is no rotation around the Ru–S bond, as it had been observed previously for the  $[\text{XW}_{11}\text{O}_{39}\{\text{Ru}(\text{DMSO})_3(\text{H}_2\text{O})\}]^{6-}$  compounds (X = Si, Ge)).<sup>39</sup> Similarly, the observation of five singlets of relative intensity 1:1:1:1:2 for **2** suggests that an  $\{\text{Os}(\text{DMSO})_3\}^{2+}$  fragment is grafted onto the polyoxometallic framework.<sup>40</sup> As in the case of  $[\alpha\text{-PW}_{11}\text{O}_{39}\{\text{Ru}(\eta^6\text{-}p\text{-cym})(\text{H}_2\text{O})\}]^{5-}$  (**4**), the <sup>1</sup>H NMR spectrum of **3** displays only one set of signals for the *p*-cymene ligand (different from that of the starting material) and the aromatic protons are all inequivalent.<sup>13</sup> These <sup>1</sup>H NMR analyses suggest that **1**, **2**, and **3** are formed by coordination of, respectively,  $\{\text{Ru}(\text{DMSO})_3\}^{2+}$ ,  $\{\text{Os}(\text{DMSO})_3\}^{2+}$ , and  $\{\text{Os}(\eta^6\text{-}p\text{-cym})\}^{2+}$  fragments on the lacuna of  $[\alpha\text{-PW}_{11}\text{O}_{39}]^{7-}$ .

The IR spectra of the precipitates resulting from the addition of CsCl to the mother liquor after 1 h of reflux are shown in Figure 2. In the region of the M–O stretching vibrations (below 1100 cm<sup>−1</sup>), they present the same profile as Cs<sub>5</sub>[ $\alpha\text{-PW}_{11}\text{O}_{39}\{\text{Ru}(\eta^6\text{-}p\text{-cym})(\text{H}_2\text{O})\}]$  (**Cs<sub>5</sub>-4**),<sup>13</sup> the compound for which the structure had been determined by X-ray crystallography. This suggests that the oxometallic framework is the same for all compounds: the electrophilic fragments ( $\{\text{Ru}(\text{DMSO})_3\}^{2+}$ ,  $\{\text{Os}(\text{DMSO})_3\}^{2+}$ , and  $\{\text{Os}(\eta^6\text{-}p\text{-cym})\}^{2+}$ ) are bonded to two

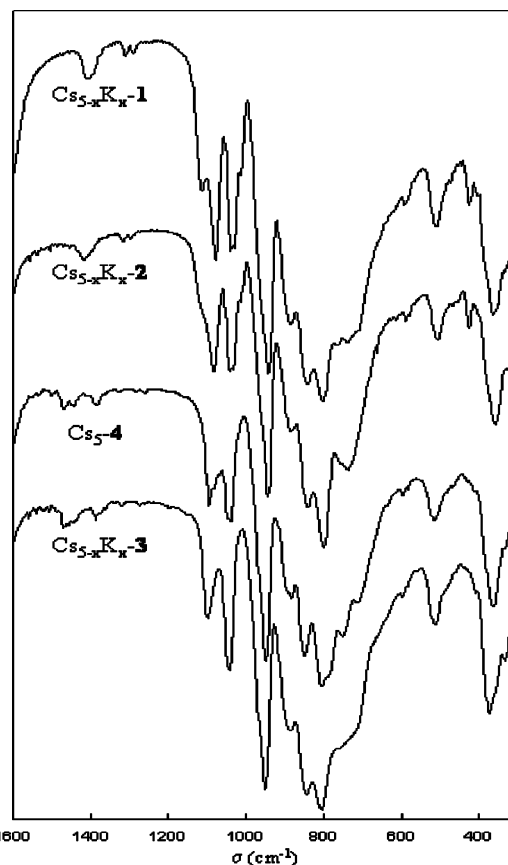


**Figure 2.** Comparison of the IR spectra of Cs<sub>5-x</sub>K<sub>x</sub>-1, Cs<sub>5-x</sub>K<sub>x</sub>-2, Cs<sub>5-x</sub>K<sub>x</sub>-3, and Cs<sub>5</sub>-4.

nonequivalent oxygen atoms of the lacuna, leading to the loss of symmetry of the parent anion  $[\alpha\text{-PW}_{11}\text{O}_{39}]^{7-}$ .<sup>41</sup> It is noteworthy that similarities in the binding properties of  $\{\text{M}(\text{DMSO})_3\}^{2+}$  (M = Ru, Os) fragments onto a POM had already been evidenced by Neumann through the formation of  $[\{\text{M}^{\text{II}}(\text{DMSO})_3\}\text{Mo}_7\text{O}_{24}]^{4-}$  (M = Ru, Os).<sup>42</sup> The similarity between the IR spectra of Cs<sub>5-x</sub>K<sub>x</sub>-1, Cs<sub>5-x</sub>K<sub>x</sub>-2, Cs<sub>5-x</sub>K<sub>x</sub>-3, and Cs<sub>5</sub>-4, the reactivity of the starting Ru<sup>II</sup> and Os<sup>II</sup> precursors in water, and the X-ray structures of **4** and of the  $[\beta\text{-XW}_{11}\text{O}_{39}\{\text{Ru}(\text{DMSO})_3(\text{H}_2\text{O})\}]^{6-}$  compounds (X = Si, Ge) synthesized by Kortz (but incorrectly described as the  $\alpha$  isomers),<sup>39</sup> all suggest that the Ru<sup>II</sup> and Os<sup>II</sup> metals achieve an 18-electron environment by coordination to an aqua ligand. It is noteworthy that, in this study, we obtained the  $\alpha$  isomers of  $[\text{PW}_{11}\text{O}_{39}\{\text{Ru}(\text{DMSO})_3(\text{H}_2\text{O})\}]^{5-}$  and  $[\text{PW}_{11}\text{O}_{39}\{\text{Os}(\text{DMSO})_3(\text{H}_2\text{O})\}]^{5-}$ . Indeed, on one hand, it is very unlikely that the  $[\alpha\text{-PW}_{11}\text{O}_{39}]^{7-}$

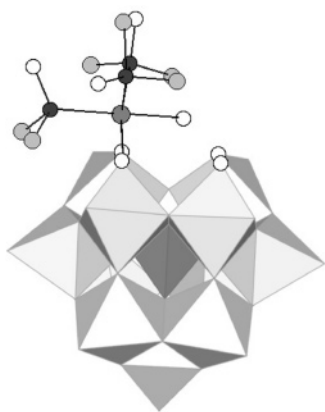


**Figure 3.** Molecular structure proposed for **1** and **2**.

anion would have isomerized in water into the  $\beta_3$  form, before the grafting of  $\{M(\text{DMSO})_3(\text{H}_2\text{O})\}^{2+}$  ( $M = \text{Ru}, \text{Os}$ ).<sup>43</sup> On the other hand, the profile of the IR spectrum of **Cs**<sub>5-x</sub>**K**<sub>x</sub>**-1** and **Cs**<sub>5-x</sub>**K**<sub>x</sub>**-2** in the region below 450 cm<sup>-1</sup> confirms the formation of an  $\alpha$  form.<sup>44</sup> The structure proposed for **1** and **2** is thus depicted in Figure 3.

Consequently, throughout this first Experimental Section, the bidentate role of the [ $\alpha$ -PW<sub>11</sub>O<sub>39</sub>]<sup>7-</sup> polyanion toward  $\{\text{Ru}(\eta^6\text{-arene})\}^{2+}$  moieties was extended to the  $\{\text{Ru}(\text{DMSO})_3\}^{2+}$  fragment and to the  $\{\text{Os}(\eta^6\text{-}p\text{-cym})\}^{2+}$  and  $\{\text{Os}(\text{DMSO})_3\}^{2+}$  analogues.

The similarities between the structures of [ $\alpha$ -PW<sub>11</sub>O<sub>39</sub>]<sup>7-</sup> $\{M(\text{DMSO})_3(\text{H}_2\text{O})\}^{2+}$  ( $M = \text{Ru}, \text{Os}$ ) and [ $\alpha$ -PW<sub>11</sub>O<sub>39</sub>]<sup>7-</sup> $\{M(\eta^6\text{-arene})(\text{H}_2\text{O})\}^{2+}$  ( $M = \text{Ru}, \text{Os}$ ) are striking: one structure derives from the other by the formal replacement of the *fac*- $\{M(\text{DMSO})_3\}^{2+}$  group by the  $\{M(\eta^6\text{-arene})\}^{2+}$  fragment. Additionally, the bidentate grafting is found to be fully regioselective, leading to two enantiomeric forms whatever the nature of the grafted moiety. A theoretical study of the bidentate coordination of these metal fragments onto the lacunary POM was thus undertaken, to understand and analyze the various points commented above.

First, the coordination is studied from a fragment interaction point of view: the full [ $\alpha$ -PW<sub>11</sub>O<sub>39</sub>]<sup>7-</sup> $\{ML_3(\text{H}_2\text{O})\}^{2+}$  complex is decomposed into a lacunary POM in interaction with a  $d^6$  metal fragment. This decomposition of the complex into two simple fragments does not imply any mechanistic feature for its formation. The orbital structure of the different grafted metal fragments is thus reported, to compare their electrophilic properties; this allows a better understanding of the origin of the similarities between the *fac*- $\{M(\text{DMSO})_3\}^{2+}$  and the  $\{M$ -

$(\eta^6\text{-arene})\}^{2+}$  groups. Then, the electronic and geometric structure of [ $\alpha$ -PW<sub>11</sub>O<sub>39</sub>]<sup>7-</sup> is computed and discussed; it points out the role of geometry optimization on the orbital properties of the POM and thus on its binding ability.

Second, an energetic study of the regioselective grafting is described in the case of the [ $\alpha$ -PW<sub>11</sub>O<sub>39</sub>]<sup>7-</sup> $\{\text{Ru}(\eta^6\text{-arene})(\text{H}_2\text{O})\}^{2+}$  complex, used as a prototype entity: the three possible regioisomers resulting from the bidentate grafting of the  $\{\text{Ru}(\eta^6\text{-arene})(\text{H}_2\text{O})\}^{2+}$  are computed and compared and then the energetics of water coordination to this entity is examined.

#### 4. Qualitative Study of the Grafting: Orbital Analysis

The first step in our study was to compare the electrophilic properties of the different  $\{ML_3(\text{H}_2\text{O})\}^{2+}$  fragments grafted on the POM. We examined if simple considerations on their lowest unoccupied orbitals (LUMOs) could justify the analogy in their mode of coordination. Afterward, a study of the HOMO of the lacunary POM was carried out. Indeed, even though the POM and the metal fragment are charged species, it can be shown that the observed nonsymmetrical coordination mode is not governed by charge control: charge control coordination should occur in a symmetrical way, since the charges on atoms symmetric across the  $\sigma_d$  plane have to be identical. Additionally, charges computation shows that the largest negative charges on the POM are not located on the O of the lacuna but on bridging atoms.

**4.1. Metal Fragments:  $\{M(\text{DMSO})_3(\text{H}_2\text{O})\}^{2+}$  vs  $\{M(\eta^6\text{-C}_6\text{H}_6)(\text{H}_2\text{O})\}^{2+}$ .** To investigate the coordination analogy of ruthenium and osmium fragments in **1**, **2**, **3**, and **4**, the orbital structure of  $\{M(\text{DMSO})_3(\text{H}_2\text{O})\}^{2+}$  was compared with that of  $\{M(\eta^6\text{-C}_6\text{H}_6)(\text{H}_2\text{O})\}^{2+}$  ( $M = \text{Ru}, \text{Os}$ ) (the benzene is used here to model the arene ligand).<sup>45</sup> Since the metal fragments can be considered as electrophilic entities with respect to [ $\alpha$ -PW<sub>11</sub>O<sub>39</sub>]<sup>7-</sup>, only the LUMOs are examined. For all fragments, the energy gap between the LUMO and the LUMO+1 is found to be quite large; consequently, the LUMO+1 will play no major influence on the electrophilic orbital properties of these fragments, which are mainly described by the LUMO. The LUMOs obtained in the case of ruthenium are given in Figure 4, whereas the orbitals computed with osmium can be found in the Supporting Information. Indeed, since the LUMOs of  $\{\text{Ru}(\eta^6\text{-C}_6\text{H}_6)(\text{H}_2\text{O})\}^{2+}$  and  $\{\text{Os}(\eta^6\text{-C}_6\text{H}_6)(\text{H}_2\text{O})\}^{2+}$  and of  $\{\text{Ru}(\text{DMSO})_3(\text{H}_2\text{O})\}^{2+}$  and  $\{\text{Os}(\text{DMSO})_3(\text{H}_2\text{O})\}^{2+}$ , respectively, are almost identical, only the ruthenium moieties are described.

The LUMOs of both  $\{\text{Ru}(\eta^6\text{-C}_6\text{H}_6)(\text{H}_2\text{O})\}^{2+}$  and  $\{\text{Ru}(\text{DMSO})_3(\text{H}_2\text{O})\}^{2+}$  are found to be highly similar: they are both metal centered, with a strong  $d_{yz}$  character, and of  $\pi$  symmetry with respect to a ligand approaching along the  $z$  axis.

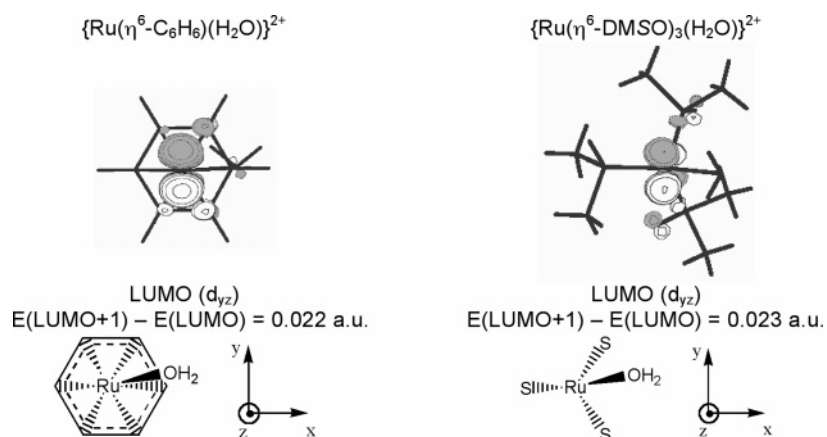


**Figure 4.** Representation of the LUMO of  $\{\text{Ru}(\eta^6\text{-C}_6\text{H}_6)(\text{H}_2\text{O})\}^{2+}$  (left) and  $\{\text{Ru}(\text{DMSO})_3(\text{H}_2\text{O})\}^{2+}$  (right) (isodensity = 0.09).

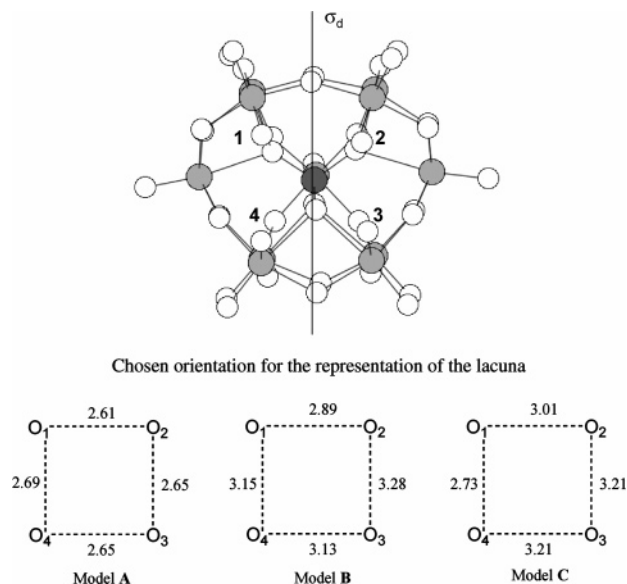


**Figure 5.** Orientation chosen for  $[\alpha\text{-PW}_{11}\text{O}_{39}]^{7-}$  and oxygen–oxygen bond distances (in angstroms) in the X-ray structures of models **A**, **B**, and **C**.

Given the similarities between their LUMOs, the binding properties of all  $\{\text{M}^{\text{II}}\text{L}_3(\text{H}_2\text{O})\}^{2+}$  fragments with respect to different nucleophiles are thus expected to be the same, in particular toward the bidentate ligands. The regioselectivity of their bidentate coordination to the lacuna of  $[\alpha\text{-PW}_{11}\text{O}_{39}]^{7-}$  was then studied by computation of the HOMO of this ligand.

**4.2. Orbital Analysis of  $[\alpha\text{-PW}_{11}\text{O}_{39}]^{7-}$ .** A lot of computational studies have been carried out on complete POMs, and they mostly investigate their structural, electronic, and magnetic properties.<sup>46</sup> Fewer results are published on the lacunary POMs,<sup>47</sup> so that very little is known on the properties of such POMs as ligands toward transition metal compounds. In this section, the analysis of the factors influencing the proper representation of the lacuna of  $[\alpha\text{-PW}_{11}\text{O}_{39}]^{7-}$  is carried out. First, the geometrical characteristics of the lacuna are described. Afterward, different models of the lacuna are examined to understand the parameters essential for the reproduction of its electronic properties.

**Discussion about the Geometry of the Lacuna.** In a first attempt to understand coordination modes, the lacunas in three different crystallographic structures containing the  $[\alpha\text{-PW}_{11}\text{O}_{39}]^{7-}$  entity are compared. The first one (called model **A**) is extracted from the structure of the complete POM  $[\alpha\text{-PW}_{12}\text{O}_{40}]^{3-}$ ,<sup>48</sup> from which one  $\{\text{WO}\}^{4+}$  fragment was removed.<sup>49</sup> The second one (**B**) derives from the X-ray structure of an  $[\alpha\text{-PW}_{11}\text{O}_{39}]^{7-}$  compound in which a  $\text{Na}^+$  cation occupies the cavity.<sup>50</sup> The last one (**C**) stems from the X-ray data of **4**,<sup>13</sup> by removal of the  $\{\text{Ru}(\eta^6\text{-p-cym})(\text{H}_2\text{O})\}^{2+}$  entity. A scheme of these geom-

etries is given in Figure 5, using the orientation presented. The oxygen atoms of the lacuna are labeled O<sub>1</sub> to O<sub>4</sub>. Both orientation and labeling will be conserved throughout the rest of this section.

It is noteworthy that a pseudoplane of symmetry ( $\sigma_d$ ) exists in the structures of **A** and **B**, even though the O<sub>1</sub>⋯O<sub>4</sub> and O<sub>2</sub>⋯O<sub>3</sub> distances are not exactly equal in the X-ray structure. In **C**, this symmetry is broken due to the coordination of the Ru fragment.

Differences up to 0.5 Å are observed for the O⋯O distances and can be easily rationalized. In the case of **C**, the shortest O⋯O distance is found between O<sub>1</sub> and O<sub>4</sub>, which are the two oxygen atoms which were initially coordinated to  $\{\text{Ru}(\eta^6\text{-p-cym})(\text{H}_2\text{O})\}^{2+}$ . In the case of **A** and **B**, the two shortest distances should be found between O<sub>1</sub>⋯O<sub>2</sub> and O<sub>3</sub>⋯O<sub>4</sub>, which happen to be connected by only one W–O–W bridge. But, among them, the distance between O<sub>3</sub> and O<sub>4</sub> is longer, because an oxygen atom of the  $[\text{PO}_4]^{3-}$  entity points between these atoms and introduces an additional repulsion; the O<sub>3</sub>⋯O<sub>4</sub> distance thus approaches the O<sub>1</sub>⋯O<sub>4</sub> and O<sub>2</sub>⋯O<sub>3</sub> distances.

**Modeling the Lacuna.** To investigate the structural features responsible for the electronic properties of the lacunary POM, two simplified models were used and compared with the complete system, using the geometry of model **B**.

First, a simple model of the lacunary POM,<sup>47b,51</sup> consisting of four hydroxo ligands, was computed. The geometry chosen to position the four fragments was directly derived from the X-ray structure of **B**. The oxygen atoms of the lacuna were kept into their initial position, and the OH bonds were directed along the O–W bonds and adjusted to the length of 1.1 Å.

Second, the calculations were undertaken on the POM deprived of both the  $\text{Na}^+$  and the central  $[\text{PO}_4]^{3-}$  core. In the case of complete Keggin anions, this model, referred to as the clathrate model, had given relatively good results in computing their electronic properties.<sup>52</sup>

The resulting HOMOs for these two fragments and for the complete lacunary POM (nonoptimized, model **B**) are given in Figure 6.

In the smaller model, the HOMO is a combination of 2p orbitals of the O atoms, which are perpendicular to the OH bonds and within the plane of the four oxygen atoms. For the larger structures, the electronic density of the orbital is spread out on different bridging and terminal oxygen atoms of the POM and in particular on the oxygen atoms of the lacuna.

In the  $(\text{OH})_4$  model, the HOMO is antisymmetrical with respect to the  $\sigma_d$  symmetry plane and mainly developed on the two oxygen atoms which are the closest in the X-ray structure, namely, O<sub>1</sub> and O<sub>2</sub>. This is not surprising, insofar as the proximity of both atoms leads to an enhancement of the antibonding interaction between the 2p orbitals and consequently increases their energy. In the clathrate model, the HOMO is

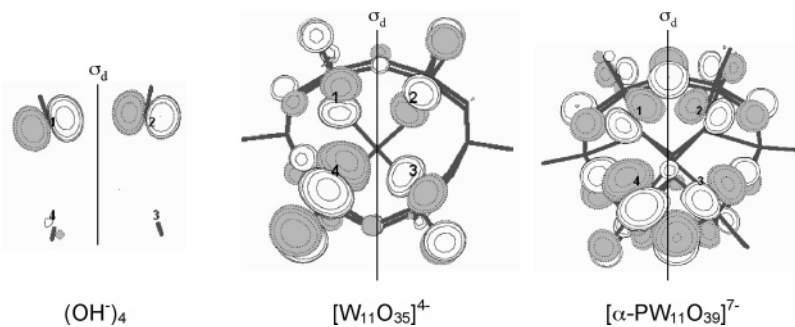


**Figure 6.** HOMO orbitals for  $(\text{OH})_4$  (isodensity = 0.08),  $[\text{W}_{11}\text{O}_{35}]^{4+}$ , and  $[\alpha\text{-PW}_{11}\text{O}_{39}]^{7-}$  derived from **B** (single point) (isodensity = 0.02).



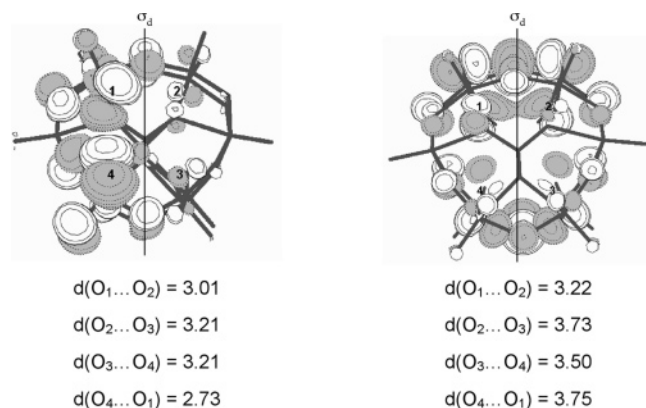


**Figure 7.** Representation of the HOMO of [ $\alpha$ -PW<sub>11</sub>O<sub>39</sub>]<sup>7-</sup> derived from **C**, single point (left) or optimized (right) (isodensity = 0.02). The corresponding O $\cdots$ O<sub>*j*</sub> distances are given in angstroms.

antisymmetric with respect to the  $\sigma_d$  plane and displays a fully antibonding combination of the 2p lone pairs of the oxygen atoms contained in the lacuna plane. On the opposite, in the presence of the central [PO<sub>4</sub>]<sup>3-</sup>, the interaction between the 2p orbitals of the oxygen atoms of the lacuna in the HOMO is not fully antibonding anymore. The HOMO is now symmetric with respect to the  $\sigma_d$  plane, and thus, the interaction between the oxygen atoms of the lost triad (O<sub>1</sub> $\cdots$ O<sub>2</sub> and O<sub>3</sub> $\cdots$ O<sub>4</sub>) is bonding, whereas it is antibonding between the other neighboring oxygen atoms (O<sub>1</sub> $\cdots$ O<sub>4</sub> and O<sub>3</sub> $\cdots$ O<sub>2</sub>).

$\pi$ -Interaction of the {ML<sub>3</sub>(H<sub>2</sub>O)}<sup>2+</sup> (M = Ru, Os) moiety would be favored between O<sub>1</sub> and O<sub>2</sub> for the (OH<sup>-</sup>)<sub>4</sub> model of **B** and could occur between any group of two adjacent oxygen atoms in the clathrate model. Only the complete anion can fully account for the regiospecific grafting of {ML<sub>3</sub>(H<sub>2</sub>O)}<sup>2+</sup>: the  $\pi$  arrangement necessary for coordination appears between either O<sub>1</sub> and O<sub>4</sub> or O<sub>2</sub> and O<sub>3</sub>, thereby provoking the loss of the C<sub>s</sub> symmetry of the POM.

Whereas the HOMO in the small (OH<sup>-</sup>)<sub>4</sub> model is (not surprisingly) developed between the closest oxygen atoms of the lacuna, a comparison of the clathrate model and of the complete POM shows that the phosphate plays an indirect but essential role in defining the symmetry of the HOMO and consequently in the coordination abilities of the POM to metallic fragments.

**Impact of Geometrical Factors on the HOMO of the Lacunary POM.** Since the (OH<sup>-</sup>)<sub>4</sub> model showed the role of the geometry of the lacuna on the aspect of the HOMO, this orbital was also computed in the case of the **C** structure, in which the O<sub>1</sub> $\cdots$ O<sub>4</sub> distance is significantly shorter, and thus the C<sub>s</sub> symmetry broken. The result is given in Figure 7. The shortening of the O<sub>1</sub> $\cdots$ O<sub>4</sub> distance leads, as expected, to a higher localization of the HOMO between the 2p orbitals of these oxygen atoms. They interact in an antibonding way and thereby enhance the asymmetric binding ability of the POM to the electrophilic metal center. Since the regiospecificity of the bidentate grafting can be accounted for with models **B** and **C**, the use of the X-ray structure of the grafted POM (**C**) is not necessary for this study, since it only enhances the localization of the HOMO.

Additionally, the lacunary POM was fully optimized and its HOMO computed. It is noteworthy that the optimization process resulted in the same final geometry whatever starting structure (**A**, **B**, or **C**) was used. As evidenced in Figure 7, optimization of the lacunary POM in the absence of a cation in the lacuna results in a strong redistribution of the electronic density on the other oxygen atoms of the cluster, and the HOMO becomes

almost symmetrical with respect to the C<sub>s</sub> symmetry plane. However, whereas the HOMOs computed on the two X-ray extracted geometries (models **B** and **C**) presented can account for the regiospecific grafting, the HOMO of a fully optimized structure does not allow us to conclude.

A closer look at the results for geometry optimization shows a clear opening of the lacuna as reflected from the O $\cdots$ O distances: they all increase by more than 0.3 Å, probably because of an electrostatic repulsion between the terminal oxygen atoms O<sub>1</sub>, O<sub>2</sub>, O<sub>3</sub>, and O<sub>4</sub>. The geometry changes due to optimization are much larger than the geometrical differences described above in the various models **A**, **B**, and **C**. Such an increase in the O $\cdots$ O distances between the oxygen atoms of the lacuna had already been observed in the literature for DFT studies of the bilacunary [ $\gamma$ -SiW<sub>10</sub>O<sub>36</sub>]<sup>8-</sup> polyoxoanion: in that case, optimization led to an increase of 0.4 Å in the distances between the oxygen atoms of the lacuna which are only separated by one {W-O-W} bridge.<sup>47b</sup>

**4.3. Conclusion on Orbital Considerations.** At this point, several aspects can be deduced from these orbital studies:

(i) All {ML<sub>3</sub>(H<sub>2</sub>O)}<sup>2+</sup> fragments (M = Ru, Os; L<sub>3</sub> =  $\eta^6$ -C<sub>6</sub>H<sub>6</sub>, *fac*-(DMSO)<sub>3</sub>) exhibit similar orbital properties, so that the electrophilic grafting on [ $\alpha$ -PW<sub>11</sub>O<sub>39</sub>]<sup>7-</sup> can be studied on either of these fragments.

(ii) The whole oxoanionic framework of [ $\alpha$ -PW<sub>11</sub>O<sub>39</sub>]<sup>7-</sup> (including the [PO<sub>4</sub>]<sup>3-</sup> moiety) must be considered to compute the HOMO, since the symmetry of this orbital, and thus its coordinating abilities, may be modified by removing part of the oxoanion.

(iii) The HOMO computed after geometry optimization of [ $\alpha$ -PW<sub>11</sub>O<sub>39</sub>]<sup>7-</sup> hardly accounts for the regiospecific grafting of {ML<sub>3</sub>(H<sub>2</sub>O)}<sup>2+</sup> moieties on the lacuna.

(iv) The bidentate and regiospecific linkage of the {ML<sub>3</sub>(H<sub>2</sub>O)}<sup>2+</sup> fragments (M = Os, Ru) can be explained by the single-point computation of the HOMO of the lacunary anion derived from the X-ray structures available for [ $\alpha$ -PW<sub>11</sub>O<sub>39</sub>]<sup>7-</sup> (models **B** and **C**).

## 5. Quantitative Study of the Different Modes of Grafting on [ $\alpha$ -PW<sub>11</sub>O<sub>39</sub>]<sup>7-</sup>

Even though regiospecific coordination of the {ML<sub>3</sub>(H<sub>2</sub>O)}<sup>2+</sup> moieties can be qualitatively understood from molecular orbital analysis, no quantitative information concerning either the energetics or geometrical data of the grafting have been obtained. These are accessible via geometry optimizations of the different complete POMs, which are exposed in the following section.

Because of the strong similarities in the electrophilic properties of the different grafted fragments we underscored in the orbital analysis, and since all species are formed in similar experimental conditions, the results of an energy study on compounds **1**, **2**, and **3** are expected to be analogous to those obtained on [ $\alpha$ -PW<sub>11</sub>O<sub>39</sub>{Ru( $\eta^6$ -C<sub>6</sub>H<sub>6</sub>)(H<sub>2</sub>O)}]<sup>5-</sup>. Therefore, due to the higher computational cost linked to the numerous degrees of freedom in [ $\alpha$ -PW<sub>11</sub>O<sub>39</sub>{M(DMSO)<sub>3</sub>(H<sub>2</sub>O)}]<sup>5-</sup> (M = Ru, Os), the energy study of the regiospecificity of the grafting was only performed on [ $\alpha$ -PW<sub>11</sub>O<sub>39</sub>{Ru( $\eta^6$ -C<sub>6</sub>H<sub>6</sub>)(H<sub>2</sub>O)}]<sup>5-</sup>.

**5.1. Competition between the Different Regioisomers.** We considered the three possible regioisomers for [ $\alpha$ -PW<sub>11</sub>O<sub>39</sub>{Ru( $\eta^6$ -C<sub>6</sub>H<sub>6</sub>)(H<sub>2</sub>O)}]<sup>5-</sup>, in which the {Ru( $\eta^6$ -C<sub>6</sub>H<sub>6</sub>)(H<sub>2</sub>O)}<sup>2+</sup> moiety is grafted either in an unsymmetrical way, between O<sub>1</sub> and O<sub>4</sub>,<sup>53</sup> or in a symmetrical way, either between O<sub>1</sub> and O<sub>2</sub> (the shorter O $\cdots$ O distance) or between O<sub>3</sub> and O<sub>4</sub> (the longer one).

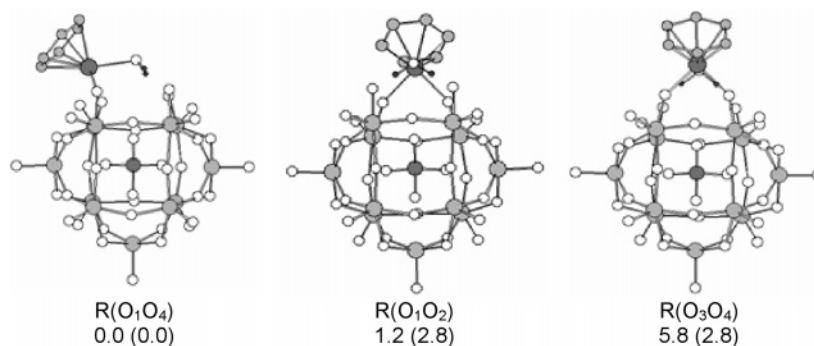


**Figure 8.** Optimized structures, labeling, and energies of the three regioisomers of  $[\alpha\text{-PW}_{11}\text{O}_{39}\{\text{Ru}(\eta^6\text{-C}_6\text{H}_6)(\text{H}_2\text{O})\}]^{5-}$ . Energies (in  $\text{kcal}\cdot\text{mol}^{-1}$ ) are given relative to the most stable isomer (values in parentheses correspond to the solvated energies). For reasons of clarity, the hydrogen atoms on the benzene ligands are not represented.

**TABLE 3: Significant Interatomic Bond Distances (in angstroms) in the X-ray Structure of 4 and in the Optimized Structures of  $\text{R}(\text{O}_1\text{O}_4)$ ,  $\text{R}(\text{O}_1\text{O}_2)$ , and  $\text{R}(\text{O}_3\text{O}_4)$  in the Gas Phase and in Solution (S)**

distance	X-ray ( $\text{O}_1\cdots\text{O}_4$ )	$\text{R}(\text{O}_1\text{O}_4)$	$\text{R}(\text{O}_1\text{O}_2)$	$\text{R}(\text{O}_3\text{O}_4)$	$\text{R}(\text{O}_1\text{O}_4)$ (S)	$\text{R}(\text{O}_1\text{O}_2)$ (S)	$\text{R}(\text{O}_3\text{O}_4)$ (S)
$\text{O}_1\cdots\text{O}_2$	3.01	2.94	2.69	3.14	3.02	2.76	3.13
$\text{O}_2\cdots\text{O}_3$	3.21	3.56	3.40	3.22	3.32	3.51	3.25
$\text{O}_3\cdots\text{O}_4$	3.21	3.14	3.37	2.77	3.23	3.41	2.82
$\text{O}_4\cdots\text{O}_1$	2.73	2.86	3.37	3.20	2.91	3.47	3.24
$\Sigma(\text{O}_i\cdots\text{O}_j)$	12.16	12.50	12.83	12.33	12.48	13.15	12.44
$\text{Ru}\cdots\text{O}_1$	2.06	2.01	2.02	4.09	2.09	2.10	4.17
$\text{Ru}\cdots\text{O}_2$	4.05	3.93	2.01	4.10	4.10	2.10	4.17
$\text{Ru}\cdots\text{O}_3$	4.16	4.05	4.13	1.99	4.18	4.28	2.08
$\text{Ru}\cdots\text{O}_4$	2.04	2.00	4.13	1.99	2.07	4.28	2.08
$\text{Ru}\cdots\text{O}_w^a$	2.08	2.10	2.09	2.10	2.15	2.12	2.14
$\text{O}_w\cdots\text{O}_{L1}^b$	2.59	2.58	2.56	2.59	2.68	2.66	2.63
$\text{O}_w\cdots\text{O}_{L2}^b$	2.63	2.59	2.56	2.59	2.68	2.66	2.65
$\text{O}_w\cdots\text{H}_1^c$		1.02	1.02	1.01	1.00	1.00	1.00
$\text{O}_w\cdots\text{H}_2^c$		1.01	1.01	1.01	1.00	1.00	1.00
$\text{H}_1\cdots\text{O}_{L1}$		1.57	1.59	1.62	1.70	1.72	1.71
$\text{H}_2\cdots\text{O}_{L2}$		1.60	1.59	1.63	1.75	1.72	1.70
$\text{W}_1\cdots\text{O}_1$	1.78	1.82	1.84	1.75	1.77	1.82	1.75
$\text{W}_2\cdots\text{O}_2$	1.72	1.76	1.84	1.75	1.75	1.82	1.75
$\text{W}_3\cdots\text{O}_3$	1.70	1.76	1.76	1.86	1.75	1.77	1.80
$\text{W}_4\cdots\text{O}_4$	1.75	1.84	1.76	1.85	1.78	1.77	1.80
$\text{Ru}\cdots\text{C}$ (avg)	2.15	2.19	2.20	2.20	2.21	2.21	2.21

<sup>a</sup>  $\text{O}_w$  = oxygen atom of the water ligand. <sup>b</sup>  $\text{O}_{L1} = \text{O}_2$  and  $\text{O}_{L2} = \text{O}_3$  for  $\text{R}(\text{O}_1\text{O}_4)$ ,  $\text{O}_{L1} = \text{O}_3$  and  $\text{O}_{L2} = \text{O}_4$  for  $\text{R}(\text{O}_1\text{O}_2)$ , and  $\text{O}_{L1} = \text{O}_1$  and  $\text{O}_{L2} = \text{O}_2$  for  $\text{R}(\text{O}_3\text{O}_4)$ . <sup>c</sup>  $\text{H}_1$  points toward  $\text{O}_{L1}$  and  $\text{H}_2$  toward  $\text{O}_{L2}$ .

These three isomers are referred to as  $\text{R}(\text{O}_1\text{O}_4)$ ,  $\text{R}(\text{O}_1\text{O}_2)$ , and  $\text{R}(\text{O}_3\text{O}_4)$  in this section. Their optimized structures as well as their relative energies are given in Figure 8.

In the gas phase, the complex which presents the lowest energy is the nonsymmetrically bonded compound  $\text{R}(\text{O}_1\text{O}_4)$ . By means of continuum solvent introduction (the solvent considered was water), the  $\text{R}(\text{O}_1\text{O}_4)$  isomer remains the most stable of the three, and its energy difference with  $\text{R}(\text{O}_1\text{O}_2)$  is slightly increased. The most stable isomer found is thus in agreement with the experimental NMR and X-ray data. However, the most surprising point is that all three isomers are close in energy, so that the less favored isomers remain energetically viable species.

Geometrical parameters relevant for the optimized and X-ray structures are given in Table 3. Comparison of the X-ray data of **4**<sup>13</sup> with the optimized structure  $\text{R}(\text{O}_1\text{O}_4)$  in the gas phase was carried out to evaluate the liability of the computational method chosen. Computed results are in good agreement with the previously published structure: the bond distances are reproduced within 0.05 Å (except for the  $\text{W}_4\cdots\text{O}_4$  distance, which is surprisingly long). As in the case of the optimization of  $[\alpha\text{-PW}_{11}\text{O}_{39}]^{7-}$ , a larger discrepancy is observed for the nonbonding distances: this can be due to intermolecular interactions in the solid state (crystal packing, counteraction effects, etc.) or to computational limitations (modelization of the *p*-cymene ligand by a benzene, highly flexible structure

leading to shallow minima, etc.). This analysis not only shows the importance of environmental effects on the obtained X-ray structure and on the experimental nonbonding distances but also confirms that, even in these conditions, the computational level chosen here leads to highly accurate bond lengths.

The Ru environment is very similar in the optimized structures of the three  $\text{R}(\text{O}_i\text{O}_j)$  regioisomers, as expected since all isomers are close in energy. The  $\text{Ru}\cdots\text{O}$  and  $\text{Ru}\cdots\text{C}$  distances differ by less than 0.03 Å. The shortest  $\text{O}_i\cdots\text{O}_j$  distances are systematically found between the oxygen atoms of the lacuna which are connected through the ruthenium atom. Additionally, the  $\text{W}-\text{O}_i$  distances can be grouped into two sets: longer ones (between 1.82 and 1.86 Å), which correspond to the  $\text{W}-\text{O}_i-\text{Ru}$  bridges, and shorter ones (between 1.75 and 1.76 Å), which connect tungsten atoms to the terminal oxygen atoms of the lacuna which are not linked to the ruthenium.

When the geometry optimization is performed in the presence of a solvent, slight variations in the different interatomic bond distances are observed. The size of the lacuna (i.e., the average  $\text{O}_i\cdots\text{O}_j$  bond distance) increases for all three isomers, and the ruthenium-POM interaction is weakened, as shown by the lengthening of the  $\text{Ru}-\text{O}$  bonds. A closer look at the structures optimized in water reveals that whereas the geometrical variations (with respect to the gas phase) are the smallest in the case of  $\text{R}(\text{O}_3\text{O}_4)$ , the opening of the lacuna is the most important in



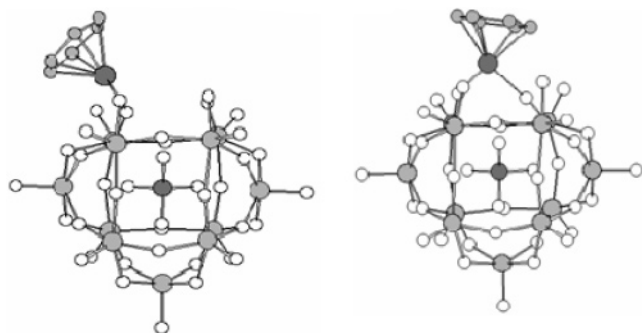


**Figure 9.** Optimized structures of [ $\alpha$ -PW<sub>11</sub>O<sub>39</sub>{Ru( $\eta^6$ -C<sub>6</sub>H<sub>6</sub>)}]<sup>5-</sup>: T2 (left) and T3 (right) (for reasons of clarity, the hydrogen atoms on the benzene ligands are not represented).

**TABLE 4: Interaction Energies (in kcal·mol<sup>-1</sup>) between [PW<sub>11</sub>O<sub>39</sub>{Ru( $\eta^6$ -C<sub>6</sub>H<sub>6</sub>)}]<sup>5-</sup> and H<sub>2</sub>O in the Different R(O<sub>*i*</sub>O<sub>*j*</sub>) Isomers Optimized in the Gas Phase, and between [Ru( $\eta^6$ -C<sub>6</sub>H<sub>6</sub>)(OH)<sub>2</sub>] and H<sub>2</sub>O in the [Ru( $\eta^6$ -C<sub>6</sub>H<sub>6</sub>)-(H<sub>2</sub>O)(OH)<sub>2</sub>] Compound Optimized in the Gas Phase**

compound	interaction energy
R(O <sub>1</sub> O <sub>4</sub> )	56.5
R(O <sub>1</sub> O <sub>2</sub> )	54.2
R(O <sub>3</sub> O <sub>4</sub> )	55.2
[Ru( $\eta^6$ -C <sub>6</sub> H <sub>6</sub> )(H <sub>2</sub> O)(OH) <sub>2</sub> ]	19.5

the case of R(O<sub>1</sub>O<sub>2</sub>). These geometrical changes could thus be linked to the large variation in the relative energy between these two isomers when including the solvent.

**5.2. Water Coordination in [ $\alpha$ -PW<sub>11</sub>O<sub>39</sub>{Ru( $\eta^6$ -C<sub>6</sub>H<sub>6</sub>)-(H<sub>2</sub>O)}]<sup>5-</sup>.** It is noteworthy that the distances between the water oxygen O<sub>w</sub> and both the ruthenium and the lacuna's oxygen atoms O<sub>2</sub> and O<sub>3</sub> for R(O<sub>1</sub>O<sub>4</sub>) reproduce particularly well the experimental data. In the optimized structure, the orientation of this aqua ligand evidences the formation of two H-bonds between the two different hydrogens and O<sub>2</sub> and O<sub>3</sub> (Figure 8). Attempts to make H-bonds using a single H bridging both oxygen atoms O<sub>2</sub> and O<sub>3</sub> were unsuccessful, insofar as they systematically converged toward the structure R(O<sub>1</sub>O<sub>4</sub>) in Figure 9.

We thus decided to investigate the coordination of the water molecule to the Ru in the grafted form from a thermodynamic point of view. First, a study of the interaction energy between the Ru and the aqua ligand in the three regioisomers R(O<sub>*i*</sub>O<sub>*j*</sub>) was performed. Then, a more detailed investigation was done for the most stable isomer R(O<sub>1</sub>O<sub>4</sub>).

The interaction energy of the water molecule with the rest of the structure was first evaluated in the gas phase as the energy difference between the absolute value of the energy of the optimized [ $\alpha$ -PW<sub>11</sub>O<sub>39</sub>{Ru( $\eta^6$ -C<sub>6</sub>H<sub>6</sub>)(H<sub>2</sub>O)}]<sup>5-</sup> R(O<sub>*i*</sub>O<sub>*j*</sub>) anion and that of the nonoptimized [ $\alpha$ -PW<sub>11</sub>O<sub>39</sub>{Ru( $\eta^6$ -C<sub>6</sub>H<sub>6</sub>)}]<sup>5-</sup> and H<sub>2</sub>O fragments (taken in the geometry of the optimized R(O<sub>*i*</sub>O<sub>*j*</sub>) isomer). As can be seen in Table 4, these energies are all above 50 kcal·mol<sup>-1</sup> but within 3 kcal·mol<sup>-1</sup>. The slight differences observed between the interaction energies of the R(O<sub>*i*</sub>O<sub>*j*</sub>) isomers cannot explain the difference between their absolute energies, since they do not vary in the same way.

These interaction energies were compared with the one obtained for the water molecule in the model complex [Ru( $\eta^6$ -C<sub>6</sub>H<sub>6</sub>)(H<sub>2</sub>O)(OH)<sub>2</sub>] (Table 4). The conformer chosen for [Ru( $\eta^6$ -C<sub>6</sub>H<sub>6</sub>)(H<sub>2</sub>O)(OH)<sub>2</sub>] was the one in which the aqua ligand makes no interaction with the hydroxo ligands, just like the water molecule in R(O<sub>*i*</sub>O<sub>*j*</sub>) which does not interact with the oxygen atoms directly bonded to the ruthenium. The interaction energy is much smaller in [Ru( $\eta^6$ -C<sub>6</sub>H<sub>6</sub>)(H<sub>2</sub>O)(OH)<sub>2</sub>] than in R(O<sub>*i*</sub>O<sub>*j*</sub>),

**TABLE 5: Energetic and Geometrical Parameters for the Optimized R(O<sub>1</sub>O<sub>4</sub>), T2, and T3**

	R(O <sub>1</sub> ···O <sub>4</sub> ) (in vacuum) <sup>b</sup>	T2 + H <sub>2</sub> O (in vacuum) <sup>b</sup>	T3 + H <sub>2</sub> O (in vacuum) <sup>b</sup>
energies <sup>a</sup>	0.0	41.1	26.6
O <sub>1</sub> ···O <sub>2</sub>	2.94	2.99	2.68
O <sub>2</sub> ···O <sub>3</sub>	3.56	3.29	3.15
O <sub>3</sub> ···O <sub>4</sub>	3.14	3.20	3.17
O <sub>4</sub> ···O <sub>1</sub>	2.86	2.73	2.78
Ru···O <sub>1</sub>	2.01	1.92	1.99
Ru···O <sub>2</sub>	3.93	4.10	2.10
Ru···O <sub>3</sub>	4.05	4.22	3.31
Ru···O <sub>4</sub>	2.00	1.93	2.10
W <sub>1</sub> ···O <sub>1</sub>	1.82	1.89	1.82
W <sub>2</sub> ···O <sub>2</sub>	1.76	1.72	1.80
W <sub>3</sub> ···O <sub>3</sub>	1.76	1.73	1.75
W <sub>4</sub> ···O <sub>4</sub>	1.84	1.89	1.82
Ru···C (avg)	2.19	2.19	2.18

<sup>a</sup> Energies are given relative to R(O<sub>1</sub>O<sub>4</sub>) in kcal·mol<sup>-1</sup>. <sup>b</sup> Distances are in angstroms.

thus indicating that, in the latter compound, the interaction of the POM framework with the aqua ligand is important and consistent with the presence of two strong hydrogen bonds, in addition to the Ru<sup>II</sup>-OH<sub>2</sub> interaction. Quantitative insights can even be obtained from the comparison of the interaction energy of the aqua ligand in the [Ru( $\eta^6$ -C<sub>6</sub>H<sub>6</sub>)(H<sub>2</sub>O)(OH)<sub>2</sub>] complex and in the R(O<sub>*i*</sub>O<sub>*j*</sub>) isomers. Indeed, it allows us to evaluate the part of the interaction energy which can be attributed to the binding to the ruthenium (around 20 kcal·mol<sup>-1</sup>, Table 4) or to the interaction of water with the POM (which thus falls to about 35 kcal·mol<sup>-1</sup>).

The structure of the nonsymmetrical [ $\alpha$ -PW<sub>11</sub>O<sub>39</sub>{Ru( $\eta^6$ -C<sub>6</sub>H<sub>6</sub>)}]<sup>5-</sup> (derived from R(O<sub>1</sub>O<sub>4</sub>)) was then fully optimized to examine how it could relax in the absence of water. A bidentate 16-electron coordination mode was optimized (named T2). A second structure (T3) was found in which the Ru completes an 18-electron environment by achieving coordination to three oxygen atoms of the lacuna as shown in Figure 9 and evidenced from the Ru···O distances given in Table 5.

From an energetical point of view, the 18-electron complex (T3) is much more stable than the 16-electron one (T2), with the energy difference being 14.5 kcal·mol<sup>-1</sup>. Decoordination of water from R(O<sub>1</sub>O<sub>4</sub>), which leads to the formation of T3, is found to be highly endothermic (26.6 kcal·mol<sup>-1</sup>), suggesting that the dehydration of R(O<sub>1</sub>O<sub>4</sub>) is disfavored. Relating these energy values to experimental behavior is both tempting and frustrating. Indeed, under photochemical irradiation, and in the presence of DMSO, **4** evolves into [ $\alpha$ -PW<sub>11</sub>O<sub>39</sub>{Ru<sup>II</sup>(DMSO)}]<sup>5-</sup>, by decoordination of the arene and aqua ligands. However, no dehydrated (like T3) or deareneated intermediates could be evidenced, because of their fast evolution in solution. Therefore, it is difficult to say which ligand leaves first and whether a T3 type compound is formed or not.

From a geometrical point of view, the coordination of Ru in T2 is very similar to that observed in R(O<sub>1</sub>O<sub>4</sub>) (disregarding, of course, the removal of the aqua ligand). However, in T2, shorter Ru-O<sub>*i*</sub> bonds (*i* = 1, 4), together with longer corresponding W-O<sub>*i*</sub> bonds (*i* = 1, 4), are characteristic of the unsaturated electronic configuration of the Ru. On the other hand, longer Ru···O nonbonding distances, together with a larger O<sub>3</sub>O<sub>4</sub>Ru angle (107.8° for T2 vs 101.3° for R(O<sub>1</sub>O<sub>4</sub>)), evidence the absence of tilting of the Ru fragment toward the center of the lacuna.

Comparing T3 and R(O<sub>1</sub>O<sub>4</sub>) is especially insightful since in both complexes the Ru is hexacoordinated and presents an 18-

electron environment. In T3, the metal exhibits a genuine tridentate mode of coordination to the lacuna, which differs from the bidentate or pentadentate (as in  $[\alpha\text{-PW}_{11}\text{O}_{39}\{\text{TiCp}\}]^{4-}$  or  $[\alpha\text{-PW}_{11}\text{O}_{39}\{\text{Ru}(\text{DMSO})\}]^{5-}$ ) coordination modes described so far in the literature. T3 formally derives from  $\text{R}(\text{O}_1\text{O}_4)$  by replacing the water molecule by one oxygen atom of the lacuna.

Comparing the structures of T2, T3, and  $\text{R}(\text{O}_1\text{O}_4)$  allows a better understanding of the distortion abilities of the lacuna. In T3, coordination to three oxygen atoms (in a quasi-equivalent way since the Ru–O bond distances are between 1.99 and 2.10 Å) is achieved by shortening the  $\text{Ru}\cdots\text{O}_2$  distance (and lengthening the corresponding  $\text{W}\cdots\text{O}_2$  bond) in comparison to T2. For all compounds, the  $\text{O}_1\cdots\text{O}_4$  distance remains roughly constant due to Ru coordination to these two atoms. The variation of the  $\text{O}_3\cdots\text{O}_4$  distance is also found to be insignificant, which might be a consequence of the presence of an oxygen atom of the  $[\text{PO}_4]^{3-}$  core pointing between these two atoms (and thus inhibiting a closer contact). Adaptation of the lacuna to the desired coordination of the grafted fragment is thus achieved by the flexibility of the  $\text{O}_1\cdots\text{O}_2$  and  $\text{O}_2\cdots\text{O}_3$  distances.

**5.3. Conclusion.** It is noteworthy that quantitative results consistent with experimental data were found for the regioselective grafting of  $\{\text{Ru}(\eta^6\text{-arene})\}^{2+}$  to the POM. It is believed, given the experimental formation of the compounds, and the orbital analysis carried out first, that these conclusions can be extended to the  $\{\text{Ru}(\text{DMSO})_3\}^{2+}$  adduct, as well as their osmium analogues. The study of water coordination in  $[\alpha\text{-PW}_{11}\text{O}_{39}\{\text{Ru}(\eta^6\text{-C}_6\text{H}_6)(\text{H}_2\text{O})\}]^{5-}$  confirms that the aqua ligand is strongly bound to the  $\text{Ru}^{\text{II}}$ , which can be ascribed to the presence of two hydrogen bonds. These results give better insight on the role of the sixth ligand on the structure and occurrence of the bidentate mode of coordination.

The small energy difference between the various regioisomers of  $[\alpha\text{-PW}_{11}\text{O}_{39}\{\text{Ru}(\eta^6\text{-C}_6\text{H}_6)(\text{H}_2\text{O})\}]^{5-}$  led us to examine the impact of the exact nature of the ligands by studying the grafting of the  $\{\text{Ru}(\text{DMSO})_n\}^{2+}$  fragments ( $n = 1, 3$ ) on  $[\text{PW}_{11}\text{O}_{39}]^{7-}$ . In particular, the experimentally observed decoordination of DMSO in **1**<sup>2a</sup> is computationally studied; this study will be exposed in due time.

## 6. Conclusion and Perspectives

In this article, the investigation of the bidentate coordination of ruthenium and osmium fragments toward the lacunary  $[\alpha\text{-PW}_{11}\text{O}_{39}]^{7-}$  heteropolyoxoanion was performed.

Several novel heteropolyoxometalates have been synthesized:  $[\alpha\text{-PW}_{11}\text{O}_{39}\{\text{M}(\text{DMSO})_3(\text{H}_2\text{O})\}]^{5-}$  ( $\text{M} = \text{Ru}, \text{Os}$ ) and  $[\alpha\text{-PW}_{11}\text{O}_{39}\{\text{Os}(\eta^6\text{-}p\text{-cym})(\text{H}_2\text{O})\}]^{5-}$ . In these compounds, as in the  $[\alpha\text{-PW}_{11}\text{O}_{39}\{\text{Ru}(\eta^6\text{-}p\text{-cym})(\text{H}_2\text{O})\}]^{5-}$  complex, the metal fragments are coordinated to two oxygen atoms of the lacuna which are not symmetric with respect to the  $C_s$  plane of  $[\alpha\text{-PW}_{11}\text{O}_{39}]^{7-}$ . The regioselectivity of these reactions can be accounted for by a theoretical approach:

(i) First, on a molecular orbital analysis basis, the LUMOs of the  $d^6$  metal fragments are found to be similar and their bidentate and regioselective linkage can be explained by the single-point computation of the HOMO of the lacunary anion derived from the X-ray structures available for  $[\alpha\text{-PW}_{11}\text{O}_{39}]^{7-}$ .

(ii) Second, the regioisomer formed experimentally after coordination of a  $\{\text{Ru}(\eta^6\text{-C}_6\text{H}_6)(\text{H}_2\text{O})\}^{2+}$  fragment on the lacuna is also found computationally to be the most stable of the three, in the gas phase as well as in solution, but by less than 3 kcal·mol<sup>-1</sup>.

(iii) Third, the water molecule in  $[\alpha\text{-PW}_{11}\text{O}_{39}\{\text{Ru}(\eta^6\text{-}p\text{-cym})(\text{H}_2\text{O})\}]^{5-}$  is found to be strongly coordinated to the metal

fragment, since decoordination of this water ligand can only be partially compensated by coordination to additional O atoms of the lacuna.

As a conclusion, this work underscores the versatility of the  $[\alpha\text{-PW}_{11}\text{O}_{39}]^{7-}$  ligand, which experimentally allows both bi- and pentadentate coordination modes but for which tricoordination can also be evidenced by means of a computational study.

**Acknowledgment.** The authors thank Dr. René Thouvenot for the fruitful discussions on the NMR spectra and Liselotte Bouquerel, student of the pre-masters program of the Ecole Normale Supérieure, for her participation in the synthesis of compounds **2** and **3**. Calculations have been performed on the IBM SP4 calculator at CCR (Université Paris VI, Paris, France), CINES (Montpellier, France), and IDRIS (Orsay, France).

**Supporting Information Available:** <sup>13</sup>C–<sup>1</sup>H HSQC NMR spectrum of **1**; <sup>1</sup>H and <sup>31</sup>P NMR spectra of **3**; representation of the LUMOs of  $\{\text{Os}(\text{DMSO})_3(\text{H}_2\text{O})\}^{2+}$  and  $\{\text{Os}(\eta^6\text{-C}_6\text{H}_6)(\text{H}_2\text{O})\}^{2+}$ . This material is available free of charge via the Internet at <http://pubs.acs.org>.

## References and Notes

- (1) (a) Anastas, P. T.; Warner, J. C. *Green Chemistry: Theory and Practice*; Oxford University Press: Oxford, U.K., 1998. (b) Lancaster, M. *Green Chemistry, An Introductory Text*; Royal Society of Chemistry: Cambridge, U.K., 2002. (c) Sheldon, R. A. *Green Chem.* **2005**, *5*, 267.
- (2) (a) Herrmann, W. A.; Kohlpaintner, C. W. *Angew. Chem., Int. Ed. Engl.* **1993**, *32*, 1524. (b) Cornils, B.; Herrmann, W. A. *Aqueous-Phase Organometallic Catalysis: Concepts and Applications*; Wiley-VCH: Weinheim, Germany, 1998.
- (3) Kuntz, E. G. *Chemtech* **1987**, *17*, 570.
- (4) Comils, B.; Wiebus, E. *Chemtech* **1995**, *25*, 33.
- (5) (a) Sheldon, R. A.; Maat, L.; Papadogianakis, G. U.S. Patent 5,536,874, 1996, to Hoechst Celanese Corp. (b) Papadogianakis, G.; Maat, L.; Sheldon, R. A. *J. Chem. Technol. Biotechnol.* **1997**, *70*, 83. (c) Ten Brink, G. J.; Arends, I. W. C. E.; Sheldon, R. A. *Science* **2000**, *287*, 1636. (d) Verspui, G.; Elbertse, G.; Sheldon, F. A.; Hacking, M. A. P. J.; Sheldon, R. A. *Chem. Commun.* **2000**, 1363. (e) Ten Brink, G. J.; Arends, I. W. C. E.; Sheldon, R. A. *Adv. Synth. Catal.* **2002**, *344*, 355. (f) Sheldon, R. A.; Papadogianakis, G. In *Aqueous-Phase Organometallic Catalysis*; Cornils, B.; Herrmann, W. A., Eds.; Wiley-VCH: Weinheim, Germany, 2004; pp 473–480.
- (6) Shirakawa, S.; Shimizu, S.; Sasaki, Y. *New J. Chem.* **2001**, *25*, 777.
- (7) Liang, H.-G.; Das, S. K.; Galvan, J. R.; Sato, S. M.; Zhang, Y.; Zakharov, L. N.; Rheingold, A. L. *Green Chem.* **2005**, *6*, 410.
- (8) (a) Pope, M. T. *Hetero and Isopoly Oxometalates*; Springer-Verlag: Berlin, Germany, 1983. (b) Hill, C. L.; Brown, R. B. *J. Am. Chem. Soc.* **1986**, *108*, 536. (c) Pope, M. T.; Müller, A. *Angew. Chem., Int. Ed. Engl.* **1991**, *30*, 56. (d) Hill, C. L.; Prosser-McCarthy, C. M. *Coord. Chem. Rev.* **1995**, *143*, 407. (e) Gouzerh, P.; Proust, A. *Chem. Rev.* **1998**, *98*, 77. (f) Neumann, R. *Prog. Inorg. Chem.* **1998**, *47*, 317. (g) Müller, A.; Peters, F.; Pope, M. T.; Gatteschi, D. *Chem. Rev.* **1998**, *98*, 239. (h) Katsoulis, D. E.; Tausch, V. S.; Pope, M. T. *Inorg. Chem.* **1987**, *26*, 215.
- (9) (a) Hill, C. L. *Angew. Chem., Int. Ed.* **2004**, *43*, 402. (b) Cadot, E.; Pilette, M.-A.; Marrot, J.; Sécheresse, F. *Angew. Chem., Int. Ed. Engl.* **2003**, *42*, 2173. (c) Szani, G.; Pope, M. T. *Dalton Trans.* **2004**, 1989. (d) Keita, B.; Mbomekalle, I.-M.; Nadjo, L.; Anderson, T. M.; Hill, C. L. *Inorg. Chem.* **2004**, *43*, 3257. (e) Bi, L.-H.; Reicke, M.; Kortz, U.; Keita, B.; Nadjo, L.; Clark, R. J. *Inorg. Chem.* **2004**, *43*, 3915. (f) Jabbour, D.; Keita, B.; Mbomekalle, I.-M.; Nadjo, L.; Kortz, U. *Eur. J. Inorg. Chem.* **2004**, 2036. (g) Dablemont, C.; Proust, A.; Afonso, C.; Fournier, F.; Tabet, J.-C. *Inorg. Chem.* **2004**, *43*, 3514. (h) Ruhlmann, L.; Canny, J.; Vaissermann, J.; Thouvenot, R. *J. Chem. Soc., Dalton Trans.* **2004**, 794.
- (10) Ho, R. K. C.; Klemperer, W. G. *J. Am. Chem. Soc.* **1978**, *100*, 6772.
- (11) Wei, X.; Dickman, M. H.; Pope, M. T. *Inorg. Chem.* **1997**, *36*, 130.
- (12) (a) Noata, T.; Takaya, H.; Murahashi, S.-I. *Chem. Rev.* **1998**, *98*, 2599. (b) Murahashi, S.-I.; Komiya, N. *Modern Oxidation Methods*; Wiley-VCH Verlag: Weinheim, Germany, 2004, 165–191. (c) Kuehn, F. E.; Fischer, R. W.; Herrmann, W. A.; Weskamp, T. *Transition Metals in Organic Synthesis*, 2nd ed.; Wiley-VCH Verlag: Weinheim, Germany, 2004; Vol. 2, pp 427–436. (d) Gladiali, S.; Alberico, E. *Transition Metals in Organic Synthesis*, 2nd ed.; Wiley-VCH Verlag: Weinheim, Germany,



2004; Vol. 2, pp 145–166. (e) Komiya, S.; Hirano, M. *Ruthenium in Organic Synthesis*; Wiley-VCH Verlag: Weinheim, Germany, 2004; pp 345–366.

(13) Artero, V.; Laurencin, D.; Villanneau, R.; Thouvenot, R.; Herson, P.; Gouzerh, P.; Proust, A. *Inorg. Chem.* **2005**, *44*, 2826.

(14) Rong, C.; Pope, M. T. *J. Am. Chem. Soc.* **1992**, *114*, 2932.

(15) Bagno, A.; Bonchio, M.; Sartorel, A.; Scorrano, G. *Eur. J. Inorg. Chem.* **2000**, 17.

(16) Contant, R. *Can. J. Chem.* **1987**, *65*, 570.

(17) (a) Evans, I. P.; Spencer, A.; Wilkinson, G. *J. Chem. Soc., Dalton Trans.* **1973**, 204. (b) Alessio, E.; Mestroni, G.; Nardin, G.; Attia, W. M.; Calligaris, M.; Sava, G.; Zorzet, S. *Inorg. Chem.* **1988**, *27*, 4099. (c) Mercer, A.; Trotter, J. J. *J. Chem. Soc., Dalton Trans.* **1975**, 2480.

(18) Antonov, P. G.; Kukushkin, Y. N.; Konnov, V. I.; Kostikov, Y. P. *Koord. Khim.* **1980**, *6*, 1585.

(19) (a) Arthur, T.; Stephenson, T. A. *J. Organomet. Chem.* **1981**, *208*, 369. (b) Cabeza, J. A.; Maitlis, P. M.; *J. Chem. Soc., Dalton Trans.* **1985**, 573.

(20) Scott, A. P.; Radom, L. *J. Phys. Chem.* **1996**, *100*, 16502.

(21) (a) When the stoichiometric mixture of *fac*-[RuCl<sub>2</sub>(DMSO)<sub>3</sub>-(DMSO)] and [ $\alpha$ -PW<sub>11</sub>O<sub>39</sub>]<sup>7-</sup> is refluxed for 1 day, signals characteristic of [ $\alpha$ -PW<sub>11</sub>O<sub>39</sub>{Ru(DMSO)}]<sup>5-</sup> ( $\delta$ (P) = -10.89 ppm,  $\delta$ (H) = 3.33 ppm) appear on the <sup>1</sup>H and <sup>31</sup>P NMR spectra of the solution (see refs 14 and 15) and both **1** and [ $\alpha$ -PW<sub>11</sub>O<sub>39</sub>{Ru(DMSO)}]<sup>5-</sup> are present at about the same concentration; however, after several days of reflux, only a slight increase in the concentration of [ $\alpha$ -PW<sub>11</sub>O<sub>39</sub>{Ru(DMSO)}]<sup>5-</sup> with respect to that of **1** can be noticed. (b) Several attempts to confirm the structure proposed for **1** by recording the <sup>183</sup>W spectrum of the mother liquor (after 1 h of reflux) were unfortunately unsuccessful: on one hand, at the limit of saturation of the mother liquor, the solution was still not concentrated enough to obtain a spectrum of good quality (it is noteworthy that more than six signals appeared on the spectrum); on the other hand, by passing this solution through a Li<sup>+</sup>-form resin (Amberlyst-15) to increase the solubility of the anion, a greater number of byproducts was observed.

(22) By continuing the reflux of the mother liquor for several hours, the partial transformation of **3** into another species **3c** ( $\delta$ (P<sub>3c</sub>) = -13.12 ppm) was observed. According to the studies concerning the evolution of solutions of **4** under reflux (see ref 13), it is likely that **3c** is the complex [ $\alpha$ -PW<sub>11</sub>O<sub>39</sub>{Os( $\eta^6$ -*p*-cym)}<sub>2</sub>{WO<sub>2</sub>}]<sup>8-</sup>.

(23) In a certain number of cases, the precipitation by cesium chloride led to the simultaneous formation of **3** and of another unidentified compound **3b**, which appears to be an osmium-arene derivative of [ $\alpha$ -PW<sub>11</sub>O<sub>39</sub>]<sup>7-</sup>: the <sup>1</sup>H NMR signature of compound **3b** in D<sub>2</sub>O is composed of one set of signals relative to the *p*-cymene ligand, and its <sup>31</sup>P NMR signal appears at  $\delta$ (P<sub>3b</sub>) = -12.50 ppm. Precipitation thus leads to the evolution of **3**, in a way that cannot be explained for the moment. In some cases, fortunately, the precipitate of **3** was pure enough to record its IR spectrum, and the IR data reported here and in Figure 2 are that of an NMR-pure precipitate of Cs<sub>5-x</sub>K<sub>x</sub>-**3**.

(24) The <sup>183</sup>W NMR spectrum of the mother liquor obtained after 1 h of reflux was not recorded, insofar as the solution is not concentrated enough and evolves at room temperature, leading to the transformation of **3** into other phosphorus-containing compounds.

(25) Frisch, M. J.; Trucks, G. W.; Schlegel, H. B.; Scuseria, G. E.; Robb, M. A.; Cheeseman, J. R.; Zakrzewski, V. G.; Montgomery, J. A., Jr.; Stratmann, R. E.; Burant, J. C.; Dapprich, S.; Millam, J. M.; Daniels, A. D.; Kudin, K. N.; Strain, M. C.; Farkas, O.; Tomasi, J.; Barone, V.; Cossi, M.; Cammi, R.; Mennucci, B.; Pomelli, C.; Adamo, C.; Clifford, S.; Ochterski, J.; Petersson, G. A.; Ayala, P. Y.; Cui, Q.; Morokuma, K.; Malick, D. K.; Rabuck, A. D.; Raghavachari, K.; Foresman, J. B.; Cioslowski, J.; Ortiz, J. V.; Baboul, A. G.; Stefanov, B. B.; Liu, G.; Liashenko, A.; Piskorz, P.; Komaromi, I.; Gomperts, R.; Martin, R. L.; Fox, D. J.; Keith, T.; Al-Laham, M. A.; Peng, C. Y.; Nanayakkara, A.; Gonzalez, C.; Challacombe, M.; Gill, P. M. W.; Johnson, B.; Chen, W.; Wong, M. W.; Andres, J. L.; Gonzalez, C.; Head-Gordon, M.; Replogle, E. S.; Pople, J. A. *Gaussian 98*, revision A.7; Gaussian Inc.: Pittsburgh, PA, 1998.

(26) (a) Becke, A. D. *J. Phys. Chem.* **1993**, *98*, 5648. (b) Perdew, J. P.; Wang, Y. *Phys. Rev. B* **1992**, *45*, 13244.

(27) (a) Wadt, W. R.; Hay, P. G. *J. Chem. Phys.* **1985**, *82*, 284. (b) Hay, P. G.; Wadt, W. R. *J. Chem. Phys.* **1985**, *82*, 299. (c) Höllwarth, A.; Böhme, M.; Dapprich, S.; Ehlers, A. W.; Gobbi, A.; Jonas, V.; Köhler, K. F.; Stegmann, R.; Veldkamp, A.; Frenking, G. *Chem. Phys. Lett.* **1993**, *208*, 237. (d) Ehlers, A. W.; Böhme, M.; Dapprich, S.; Gobbi, A.; Höllwarth, A.; Jonas, V.; Köhler, K. F.; Stegmann, R.; Veldkamp, A.; Frenking, G. *Chem. Phys. Lett.* **1993**, *208*, 111.

(28) Andrae, D.; Haeusslerman, U.; Dolg, M.; Stoll, H.; Preuss, H. *Theor. Chim. Acta* **1990**, *77*, 123.

(29) *Jaguar 6.0*; Schrödinger, LLC: Portland, Oregon, 2005.

(30) (a) Tannor, D. J.; Marten, B.; Murphy, R.; Friessner, R. A.; Sitkoff, D.; Nicholls, A.; Ringnalda, M. N.; Goddard, W. A., III; Honig, B. *J. Am. Chem. Soc.* **1994**, *116*, 11875. (b) Marten, B.; Kim, K.; Cortis, C.; Friessner, R. A.; Murphy, R. B.; Ringnalda, M. N.; Sitkoff, D.; Honig, B. *J. Phys. Chem.* **1996**, *100*, 11775.

(31) (a) Lee, C.; Yang, W.; Parr, R. G. *Phys. Rev. B* **1988**, *37*, 785. (b) Becke, A. D. *Phys. Rev. A: At., Mol., Opt. Phys.* **1988**, *38*, 3098.

(32) (a) Panina, N. S.; Calligaris, M. *Inorg. Chim. Acta* **2002**, *334*, 165. (b) Calligaris, M.; Panina, N. S. *J. Mol. Struct.* **2003**, *646*, 61. (c) Alessio, E.; Serli, B.; Zangrando, E.; Calligaris, M.; Panina, N. S. *Eur. J. Inorg. Chem.* **2003**, 3160.

(33) Perdew, J. P. *Phys. Rev. B: Condens. Matter Mater. Phys.* **1986**, *33*, 8822.

(34) (a) Stener, M.; Calligaris, M. *J. Mol. Struct.* **2000**, *497*, 91. (b) Bagno, A.; Bonchio, M. *Magn. Reson. Chem.* **2004**, *42*, S79.

(35) Bermel, W.; Griesinger, C.; Kessler, H.; Wagner, G. *Magn. Reson. Chem.* **1987**, *25*, 325.

(36) Massart, R.; Contant, R.; Fruchart, J.-M.; Ciabini, J.-P.; Fournier, M. *Inorg. Chem.* **1977**, *16*, 2916.

(37) Branes, J. R.; Goodfellow, R. J. *J. Chem. Res. B* **1979**, 350.

(38) It is well-known that the dissolution in water of the *fac*-[RuCl<sub>2</sub>-(DMSO)<sub>3</sub>(DMSO)] complex quickly leads to the substitution of the weakly coordinated O-bonded DMSO ligand by a water molecule, whereas the S-bonded DMSO molecules are more strongly linked to the Ru<sup>II</sup> center and therefore stay coordinated onto the metal (see refs 17 and 37). The presence of free DMSO in the mother liquor is therefore not surprising and confirms the decoordination of the O-bonded DMSO ligand.

(39) Bi, L.-H.; Kortz, U.; Keita, B.; Nadjio, L. *J. Chem. Soc., Dalton Trans.* **2004**, 3184.

(40) It is noteworthy that, in this case, the signals corresponding to two methyl groups accidentally overlap.

(41) The DMSO ligands coordinated to the ruthenium and the osmium appear on the IR spectra of Cs<sub>5-x</sub>K<sub>x</sub>-**1** and of Cs<sub>5-x</sub>K<sub>x</sub>-**2**: two shoulders, at 1116 and 1021 cm<sup>-1</sup> for **1** and at 1119 and 1019 cm<sup>-1</sup> for **2** can be attributed, respectively, to an S–O stretching vibration of S-bonded DMSO and to C–H rocking vibrations.

(42) Khenkin, A. M.; Shimon, L. J. W.; Neumann, R. *Inorg. Chem.* **2003**, *42*, 3331.

(43) Contant, R.; Hervé, G. *Rev. Inorg. Chem.* **2002**, *22*, 63.

(44) Thouvenot, R.; Fournier, M.; Franck, R.; Rocchiccioli-Deltcheff, C. *Inorg. Chem.* **1984**, *23*, 598.

(45) The substitution of the *p*-cymene ligand by a benzene is legitimate, insofar as the grafting modes of {Ru( $\eta^6$ -C<sub>6</sub>H<sub>6</sub>)(H<sub>2</sub>O)}<sup>2+</sup> and {Ru( $\eta^2$ -*p*-cym)-(H<sub>2</sub>O)}<sup>2+</sup> on [ $\alpha$ -PW<sub>11</sub>O<sub>39</sub>]<sup>7-</sup> are the same (see ref 13).

(46) (a) Rohmer, M.-M.; Bénard, M.; Blaudeau, J.-P.; Maestre, J.-M.; Poblet, J.-M. *Coord. Chem. Rev.* **1998**, *178–180*, 1019. (b) Borshch, S. A. *Inorg. Chem.* **1998**, *37*, 3116. (c) Bridgeman, A. J.; Cavigliasso, G. *Inorg. Chem.* **2002**, *41*, 1761. (d) Laurencin, D.; Fidalgo, E. G.; Villanneau, R.; Villain, F.; Herson, P.; Pacifico, J.; Stoeckli-Evans, H.; Bénard, M.; Rohmer, M.-M.; Süß-Fink, G.; Proust, A. *Chem.–Eur. J.* **2004**, *10*, 208. (e) Zueva, E. M.; Chermette, H.; Borshch, S. A. *Inorg. Chem.* **2004**, *43*, 2834. (f) Guo, Y.-R.; Pan, Q.-J.; Wei, Y.-D.; Li, Z.-H.; Li, X. *J. Mol. Struct. (THEOCHEM)* **2004**, *676*, 55. (g) de Visser, S. P.; Kumar, D.; Neumann, R.; Shaik, S. *Angew. Chem., Int. Ed.* **2004**, *43*, 5661. (h) Lopez, X.; Poblet, J.-M. *Inorg. Chem.* **2004**, *43*, 6863. (i) Lopez, X.; de Graaf, C.; Maestre, J.-M.; Bénard, M.; Rohmer, M.-M.; Bo, C.; Poblet, J.-M. *J. Chem. Theor. Comput.* **2005**, *1*, 856.

(47) (a) Bagno, A.; Bonchio, M.; Sartorel, A.; Scorrano, G. *Chem. Phys. Chem.* **2003**, *4*, 517. (b) Musaev, D. G.; Morokuma, K.; Geletii, Y. V.; Hill, C. L. *Inorg. Chem.* **2004**, *43*, 7702. (c) Bagno, A.; Bonchio, M. *Angew. Chem., Int. Ed.* **2005**, *44*, 2023.

(48) Inman, C.; Knaust, J. M.; Keller, S. W. *Chem. Commun.* **2002**, 156.

(49) The {WO}<sup>4+</sup> fragment which was removed from the [ $\alpha$ -PW<sub>12</sub>O<sub>40</sub>]<sup>3-</sup> anion was chosen so that the distances between the oxygen atoms of the lacuna of the resulting [ $\alpha$ -PW<sub>11</sub>O<sub>39</sub>]<sup>7-</sup> were as close as possible.

(50) Honma, N.; Kusaka, K.; Ozeki, T. *Chem. Commun.* **2002**, 2896.

(51) Bagno, A.; Bonchio, M. *Eur. J. Inorg. Chem.* **2002**, 1475.

(52) (a) Day, V. W.; Klempner, W. G. *Science* **1985**, *228*, 533. (b) Maestre, J. M.; López, X.; Bo, C.; Poblet, J.-M.; Casañ-Pastor, N. M. *J. Am. Chem. Soc.* **2001**, *123*, 3749. (c) López, X.; Maestre, J. M.; Bo, C.; Poblet, J.-M. *J. Am. Chem. Soc.* **2001**, *123*, 9571. (d) Poblet, J.-M.; López, X.; Bo, C. *Chem. Soc. Rev.* **2003**, *32*, 297.

(53) The enantiomer resulting from the grafting of the {Ru( $\eta^6$ -C<sub>6</sub>H<sub>6</sub>)-(H<sub>2</sub>O)}<sup>2+</sup> fragment on atoms O<sub>2</sub> and O<sub>3</sub> was not studied.